A reappraisal of igneous emplacement mechanisms: evidence from deformation structures, Trachyte Mesa intrusion, Henry Mountains, Utah

*Penelope I. R. Wilson[1], Kenneth J. W. McCaffrey[2], Robert W. Wilson[3], and Ian Jarvis[1]

[1] School of Geography, Geology and the Environment, Kingston University London, Kingston upon Thames KT1 2EE, UK

[2] Department of Earth Sciences, Durham University, Science Labs, Durham DH1 3LE, UK

[3] BP Exploration Operating Company Ltd., Chertsey Road, Sunbury on Thames TW16 7LN, UK

Corresponding author contact details–

Email address: penelope.small@gmail.com (or p.wilson@kingston.ac.uk)

Postal address: 32 Auckland Road, Kingston-upon-Thames KT1 3BG, UK

Telephone number: +44 (0)7809 826049

Co-author email addresses:

k.j.w.mccaffrey@durham.ac.uk

woody.wilson@uk.bp.com

i.jarvis@kingston.ac.uk

Abstract

Deformation structures in host rocks to high level igneous intrusions potentially record how magma is emplaced and accommodated within the shallow crust. Trachyte Mesa, a small intrusion in the Henry Mountains, Utah, is comprised of a series of stacked sheets. New structural analysis of the kinematic, spatial and temporal distribution of deformation structures in the host rocks to the intrusion has enabled the recognition of three distinct phases, interpreted to represent pre- (Phase 1), syn- (2A and 2B), and late-stage- (3) emplacement deformation. In this paper we present a new 5 stage model for the emplacement of Trachyte Mesa, following a two-stage growth mechanism for individual sheets, with radial growth of a thin sheet followed by vertical inflation. Syn-emplacement structures are localised to the intrusion lateral margins: prolific deformation bands widespread over the margin; and dip-slip faults restricted to the tips of individual sheets due to strain localisation during vertical inflation. Magma preferentially exploited these faults, initiating sill climbing. The order in which sheets are stacked impacts on the intrusion geometry and associated deformation. Our results offer new insights into the incremental intrusion geometries of high level magmatic bodies and the potential impact of their emplacement on surrounding sedimentary rocks.

Keywords:

Deformation Bands; Faults; Intrusion; Sill; Laccolith; Emplacement Mechanism

1. Introduction

High-level sill and laccolith complexes are an important part of sub-volcanic plumbing systems in which magma is emplaced as a series of sub-horizontal tabular sheet-like intrusions (Cruden and McCaffrey, 2001). Most studies of magmatic intrusions have concentrated on their geometry and internal architecture (Du Toit, 1920; Thompson, 2004; Thompson and Hutton, 2004; Thompson and Schofield, 2008; Schofield et al., 2012); whilst few have paid particular attention to emplacement-related deformation structures in the host rock. Yet these potentially record how magma is accommodated within the crust, shedding light on the so-called 'space problem' (Hutton, 1996, 1997; Tikoff et al., 2013; Wilson et al., In Prep.).

Mounting evidence suggests that many high-level crustal intrusions (both plutonic and small-scale satellite intrusions) are emplaced and grow through incremental addition of small volumes of magma (e.g. Pitcher, 1970; Mahan et al., 2003; Glazner et al., 2004; Morgan et al., 2008). Furthermore, recent studies have shown that tabular intrusions are often emplaced by the amalgamation of magma fingers, sheets and lobes (Pollard et al., 1975; Horsman et al., 2005; Stevenson et al., 2007a; Morgan et al., 2005, 2008; Schofield et al., 2010). This internal architecture has been resolved by a number of different methods, including magnetic and macroscopic fabric studies (de Saint Blanquat and Tikoff, 1997; Horsman et al., 2005; Stevenson et al., 2007b), field mapping of internal contacts (Morgan et al., 2008; Magee et al., 2012) and geochronology (Coleman et al., 2004; Westerman et al., 2004). A few authors (e.g. Johnson and Pollard, 1973; Jackson and Pollard, 1990; Morgan et

al., 2008) have studied how the host rocks deform as intrusions grow, crystallize and ultimately cool to ambient temperatures.

Hunt (1953) outlined three general emplacement models for high level intrusions: (1) radial growth only, with magma emplaced at a constant thickness and country rocks displaced both vertically and laterally (i.e. a “bulldozing” mechanism; Model B of Hunt, 1953, fig. 70, p. 142); (2) two-stage growth, comprising radial growth of a thin sheet followed by dominantly vertical growth and associated vertical uplift of the overriding host rocks (i.e. a “two-stage growth” mechanism; Model A of Hunt, 1953); and (3) simultaneous vertical and horizontal growth (Model C of Hunt, 1953). Various hybrid models have since been described following increased understanding of the nature of intrusive geometries, and evidence that bodies are commonly comprised by a number of smaller sheets and finger-like-lobes (e.g. Christmas-tree or Cedar-tree laccoliths; Corry, 1988). Deformation structures associated with emplacement are strongly linked to the mechanism of emplacement (Corry, 1988, figs 14–16, pp. 16–17); however, few studies have specifically targeted these structures in detail.

In this paper, we present a new structural analysis of the kinematic, spatial and temporal distribution of deformation structures in the host rocks to the Trachyte Mesa intrusion, a small satellite intrusion to the Mount Hillers intrusive complex, Henry Mountains, Utah, U.S.A. (Fig. 1). By integrating the host rock structures with the sequential intrusion history and building on previous studies (e.g. Gilbert, 1877; Johnson and Pollard, 1973; Morgan et al., 2008; Wetmore et al., 2009), we have created a new improved model for the emplacement of Trachyte Mesa. The results offer new insights into the incremental

intrusion geometries of high level magmatic bodies and the potential impact of their emplacement on surrounding sedimentary rocks.

2. Geological Setting

2.1. Henry Mountains

The Henry Mountains, located in SE Utah on the Colorado Plateau (Fig. 1a), are a type locality for the study of igneous intrusions and their emplacement. It was here that Gilbert (1877) famously first described and named laccoliths (coining the term “laccolite”; Gilbert, 1896) in terms of their modes of formation rather than their geometry. Accordingly, laccoliths are formed as a result of magma that “insinuated itself between two strata, and opened for itself a chamber by lifting all the superior beds” (Gilbert, 1877). Since the ground-breaking work of Gilbert, undertaken during an expedition to the Henry Mountains as part of the Powell Survey along the Green and Colorado Rivers, a number of studies have been carried out in the range (Hunt, 1953; Johnson and Pollard, 1973; Jackson and Pollard, 1988; Nelson and Davidson, 1993; Habert and de Saint Blanquat, 2004; Horsman et al., 2005; Morgan et al., 2005; de Saint-Blanquat et al., 2006; Wetmore et al., 2009; Wilson and McCaffrey, 2013).

The Henry Mountains consist of five principal peaks, each signifying a distinct intrusive centre. From north to south these are: Mt Ellen; Mt Pennell; Mt Hillers; Mt Holmes; and Mt Ellsworth (Fig. 1a). The intrusions are mid-Tertiary in age (Oligocene, 31.2 to 23.3 Ma K-Ar ages; Nelson et al., 1992), emplaced within a ~2.7 km thick section of Palaeozoic sedimentary rocks overlying Precambrian crystalline basement (Jackson and Pollard, 1988).

Most of the intrusions have a consistent dioritic composition (58–63% SiO_2; Hunt, 1953; Engel, 1959; Nelson et al., 1992). The diorite has a porphyritic texture, with dominant feldspar (An20 to An60; 20–40%) and hornblende (5–15%) phenocrysts (i.e. plagioclase-hornblende porphyry), the textural characteristics varying significantly from one intrusion to another (Hunt, 1953; Nelson et al., 1992).

The intrusions post-date minor Laramide orogenic activity (Late Cretaceous to Early Tertiary in age; Davis, 1978, 1999) on the Colorado Plateau. Although Laramide structures, such as the N–S trending Waterpocket Fold (part of the greater Circle Cliffs uplift; Davis, 1978; Jackson and Pollard, 1988; Bump and Davis, 2003) can be found locally, the strata into which the Henry Mountains intrusions are emplaced are nearly flat lying (gently dipping ~2˚ to the east; Jackson and Pollard, 1988). Lack of significant pre- and post-emplacement tectonism aids the identification of emplacement-related deformation structures and has preserved the original magmatic and solid-state fabrics within the intrusive bodies.

2.2. Trachyte Mesa

The Trachyte Mesa intrusion (also known as the “Howell laccolith” in the work of Gilbert; Hunt, 1988) is the most distal satellite intrusion of the Mount Hillers intrusive complex, located some 12 km to the NE of the central complex (11 in Fig. 1b). The intrusion has an elongate (~2.2 km long and 0.7 km wide) laccolithic geometry, trending NE–SW (Fig. 2). Thicknesses observed in cliff exposures range from 5 m to 50 m (Morgan et al., 2008), with an average thickness, estimated from magnetic and resistivity studies, of ~15 m (Wetmore et al., 2009). Various models have been suggested for the geometry and internal

architecture of the intrusion, ranging from a single domal “laccolitic” body (Gilbert, 1887; Hunt, 1953; Wetmore et al., 2009), to a series of stacked intrusive sheets and lobes (Johnson and Pollard, 1973; Morgan et al., 2005, 2008; Fig. 2d, e). In the exposures described by Morgan et al. (2008), a complex stacking history may be interpreted, with earlier sub-horizontally stacked intrusive sheets at the top of the sequence being flexed and arched by the emplacement of later sub-horizontally stacked tongue-like sheets beneath (Fig. 2d, e). These were evaluated further in the present study. Favouring the stacked intrusive sheet model, Morgan et al. (2008) questioned the use of the term “laccolith” for Trachyte Mesa, suggesting that it has features that represent a hybrid between a sill and a laccolith; however, from a geometric perspective, they agreed that laccolith is a reasonable term (i.e. upward doming at the roof of the intrusion).

The present-day local geomorphology closely resembles that of the original intrusion (Fig. 2a–b). This assertion is supported by the presence of multiple intrusion-host-rock contacts on the top and NW margins of the intrusion, although the SE margin is less well constrained (Morgan et al., 2008). The mesa has a relatively flat top with steeper NW and SE lateral margins. Where exposed, the base of the overall intrusion appears to be relatively concordant with the underlying sandstone, dipping <10° to the NW. Wetmore et al. (2009) concluded that the trend of the intrusion was controlled by a series of NE–SW trending pre-existing (Laramide?) folds, and they suggested that the axis of the intrusion may lie within a syncline. Regionally there is support for the NE–SW folding proposed by Wetmore et al. (2009); however, the local bedding and base intrusion contact exposures do not support the model for a tight syncline along the axis of the Trachyte Mesa intrusion. We note that this synclinal geometry was interpreted from magnetic data and is, therefore, potentially a non-

156 unique solution to the geophysical data acquired. The area analysed by Wetmore et al.
157 (2009) lies to the SW of the exposed intrusion geometries, and an alternative interpretation
158 for this deeper synclinal geometry at the base of the intrusion is that it represents a deeper
159 feeder system to the intrusion, which propagated from the SW. The more flat lying, NW
160 dipping monoclinal geometry of Morgan et al. (2008) is favoured here.

161

162 In contrast to the relatively flat lying stratigraphy below the intrusion, the host-rock units
163 above show significant distortion and deformation (Johnson and Pollard, 1973; Morgan et
164 al. 2008). At the NW margin of the intrusion, a clear monoclinal bending of the overlying
165 beds is apparent (Fig. 2e), which is interpreted to be the result of vertical and lateral growth
166 of the intrusion (Gilbert, 1887; Hunt, 1953; Johnson and Pollard, 1973; Morgan et al., 2008).
167 As discussed above, the intrusion is generally concordant with the Entrada Sandstone
168 Formation, within which it is emplaced (Johnson and Pollard, 1973; Morgan et al., 2008;
169 Wetmore et al., 2009). The Entrada Sandstone Formation (part of the San Rafael Group) is
170 Late Jurassic in age and is composed of a mixture of white cross-bedded sandstones,
171 reddish-brown silty sandstones, siltstones, and shale beds (Aydin, 1978). The Entrada
172 Sandstone, being highly porous, is the ideal lithology for the formation of deformation
173 bands and, as a result (along with the Lower Jurassic Navajo Sandstone, also found on the
174 Colorado Plateau and stratigraphically below the Entrada; Jackson and Pollard, 1988), has
175 been the focus of several studies on such structures (Aydin, 1978; Aydin and Johnson, 1978,
176 1983; Shipton and Cowie, 2001; Fossen et al., 2007).

177

178 Our field study focused on the southern end of the NW lateral intrusion margin (outlined in
179 Fig. 2) as this area offers the best exposure of the intrusion and its contact with overlying
180 host rocks (Fig. 2b, e). Detailed kinematic and geometrical studies were carried out at
181 numerous outcrops, regularly spaced along two approximately N–S structural transects
182 across the NW margin (TMTE and TMTW in Fig. 2c), and at additional outcrops close to
183 intrusion contacts (including area TMT3; Fig. 2c). At each structural station, a representative
184 structural dataset (including: deformation type; geometry; kinematics; phase; character)
185 was collected (minimum of 30 measurements per station; >50 in areas of high intensity
186 deformation).
187
188 **3. Intrusion Geometry**
189 Figure 3 provides an overview of the intrusion contact relationships on the NW margin
190 where we carried out our structural transects (TMTE and TMTW). Multiple sill sheets and
191 sheet terminations can be observed that appear to be stacked to create the greater
192 intrusive body (Fig. 2d, e). Along transect TMTE (Trachyte Mesa Transect East; Fig. 2c) from
193 NW to SE a distinct monoclinal geometry can be seen (Fig. 3a), both within the upper sill
194 sheets and the overriding sandstone beds. Bedding in this monocline goes from sub-
195 horizontal on the top of the mesa to dips of up to ~40° on the lateral margin (Figs 2e, 3),
196 back to sub-horizontal at the NW end. Lower sub-horizontal sill sheets are also apparent,
197 sandwiched between these upper and lower sheets in a zone of highly deformed sandstone
198 with little to no depositional characteristics preserved (Fig. 3a). A common feature of many
199 of the sill sheets is their “bulbous” to sub-vertical sheet terminations, which generally trend
200 parallel to the overall intrusion margin (*c.* NE–SW; Fig. 3). Morgan et al. (2008) provided a
201 comprehensive review of the stacked sill sheet geometries in this area.

The monoclinal geometry appears to be discontinuous along the margin. Along transect TMTW (Trachyte Mesa Transect West; Figs 2c, 3b), ~200 m SE of the outcrops described above, multiple sub-horizontal sheets can be seen stacked one on top of the other, with sheet terminations stepping back onto the top of the overall intrusive body. Furthermore, the morphology of the overriding sandstone appears more complex and step-like, mimicking the underlying sill sheet geometry (Fig. 3b). In this same area, upward-inclined sheet geometries can also be seen, which possibly reflect sill climbing during emplacement. In area TMT3 (Fig. 2c), intrusion geometries are less well exposed, however, the overlying sandstone units resemble the more step-like / terrace geometry seen along transect TMTW.

4. **Deformation Structures**

4.1. Structural types and geometry

As noted above, locally, bedding has been deformed to form a monoclinal fold across the NW lateral margin of the intrusion, with dips ranging from sub-horizontal to ~40^{o} to the NW on the steep limb (Figs 2, 4a). Deformation structures observed within the Entrada Sandstone host rock include: prolific deformation bands; dip-slip faults; and opening (Mode 1) joints (Figs 4b–d, 5). Most of the deformation bands are porosity reducing and cataclastic in character, showing small (mm- to cm-scale) offsets. There is a wide variation in deformation band orientation, with a dominant NE–SW trend, paralleling that of the intrusion (Figs 2a, 4b). Locally, small populations of dip-slip faults are observed, that trend parallel to the intrusion margin (NE–SW and ESE–WNW locally; Fig. 4c). A more widely distributed system of opening mode joints, striking both parallel and perpendicular to the intrusion margin, is also observed (Fig. 4d). These joints commonly show evidence for fluid

226 migration, with fine white carbonate precipitates and/or well-developed calcite crystals (Fig.
227 5g) on joint surfaces. Furthermore, apparent fluid-escape structures can be seen exploiting
228 joints on the top surface of the intrusion (Fig. 5h).
229
230 Various shear zones are observed within the intrusion and on the top surface (a number of
231 which were described by Morgan et al., 2008). Within the host-rock these are restricted to
232 the reddish-brown silty sandstone and shale unit that is commonly observed immediately
233 above the intrusion, and is not apparent in the more massive red sandstone units above
234 (Fig. 5b). In the upper few centimetres of individual intrusive sheets, and at the interface
235 between the intrusive sheets, a highly foliated (sub-horizontal foliation) zone occurs with
236 significant stretched plagioclase phenocrysts (see fig. 3a in Morgan et al., 2008). The shear
237 sense on structures on the top surface of the intrusion indicate a top-to-the-SE movement
238 (i.e. reflecting the outward, NW-oriented, horizontal motion of the underlying intrusive
239 sheet; Fig. 5b).
240
241 *4.2. Structural Phases*
242 Deformation structures observed within the host rocks to the intrusion may be categorised
243 into three distinct phases, according to: structural type; deformation character; geometry;
244 kinematics; spacing / intensity; and cross-cutting relationships observed in the field (Figs 4e–
245 h, 5).
246
247 Phase 1 consists of a set of deformation bands and extensional faults, trending oblique
248 (ENE-WSW) to the NE-SW trend of the intrusion (Figs 4e, 5a), and were found over a wide

area away from the intrusion. Phase 1 deformation bands are discrete and are often identified by offsets on bedding and cross-beds. Where significant offsets (cm- to m-scale) are seen, the sense of shear is largely extensional. Phase 1 structures display a low- to moderate-intensity, with spacing between 50 cm to 100 cm. However, high intensity (cm-scale spacing) ladder structures / deformation corridors also occur. Phase 1 structures are interpreted as being related to regional structure that predated the intense deformation that was associated with emplacement of the intrusion because they occur at distances away from the intrusion

Phase 2 comprises a second set of deformation bands and faults (Figs 4f–g, 5b–d, 6) that overprint the earlier Phase 1 structures. Both the deformation bands and the faults trend NE–SW, parallel to the NW lateral margin and overall trend of the intrusion. In contrast to Phase 1 deformation bands, Phase 2 structures are much more readily visible in exposures, often occurring as resistant ridges (ribbed character) standing proud of the host Entrada Sandstone (Fig. 5c). Microstructural analysis of these Phase 2 deformation bands shows them to be largely created as a result of cataclasis and compaction, with significant (almost 100%) porosity reduction along the deformation bands. The intensity (fracture density) of Phase 2 deformation bands is significantly higher than that of Phase 1, with fracture spacing in the order of 0.5 cm to 5 cm, although intensity decreases rapidly as you move off the intrusion margin.

Phase 2 deformation bands form conjugate sets with extensional offsets (Fig. 6a, b). Phase 2 faults are dip-slip in character, showing both normal and reverse movements (Fig. 4c, g), but with a common down to the NW offset (Fig. 6c-e). Unlike Phase 1 extensional faults, these often show a distinct principal slip surface (PSS; Fig. 6e), and slickenlines are commonly observed (Figs 4g, 5d). Phase 2 structures can be sub-divided further according to their cross-cutting relationships. Deformation bands (Phase 2A) are consistently cross-cut by the dip-slip faults (Phase 2B), as well as steeply dipping ladder zones (Fig. 6 c–e).

Phase 3 comprises a system of tensile joints, often infilled with calcite crystals, which overprint all other deformation structures (Figs 4h, 5e–h). The system of joints consists of two sets: a NW–SE trending set, perpendicular to the intrusion margin (Fig. 5e); and a NE–SW trending set, sub-parallel to the intrusion margin (Fig. 5f). No clear cross-cutting relationship is apparent between these two joint sets.

5. Spatial distribution of structures

As part of the fieldwork program, all structural data were georeferenced within a FieldMove™ project (Fig. 2) in order to capture their spatial distribution. FieldMove™ was chosen due to the ability to easily transfer the data between the various Move™ software programs in order to build models (3D Move™), create cross-sections of bedding data (2D Move™), and ultimately carry out kinematic modelling.

5.1. Structural transect profiles

Distinct structural domains were identified along the two structural transects (TMTW and TMTE) within the host rock that reflect both temporal and kinematic variations in deformation. The structural data at individual stations are plotted on two composite cross sections created in Move (Figs 7, 8). It is clear from these cross sections that Phase 1 deformation structures are only identifiable at more distal structural stations to the intrusion margin, and are overprinted by Phase 2A, 2B and 3 deformation structures with increased proximity to the intrusion. Phase 2 structures increase in intensity from just outboard of the intrusion margin, and onto the top surface of the intrusion. Phase 2A conjugate deformation bands appear to rotate about a horizontal axis in the vicinity of the flanking monocline (Figs 6a, 7, 8).

Bedding along the western section (TMTW) displays a stepped geometry with each step appearing to be associated with a new intrusive sill sheet (Fig. 7). Deformation structures vary across these 'stepped' zones, with Phase 2B (faults and steep ladder zones) appearing localised to sill sheet terminations (Figs 6d, 7). In contrast, bedding geometry appears simpler in the eastern cross section (TMTE), the monoclinal structure, lacking the 'steps' observed for TMTW. Accordingly, Phase 2B faults are also rare along the outcrops of transect TMTE (Fig. 8).

5.2. Variations with intrusion margin trend

Phase 2B, steep dip-slip (normal and reverse) faults are most commonly observed on the intrusion margin, associated with the tips / terminations of intrusive sheets (Fig. 6d, e). Phase 2B faults are largely observed only at structural station outcrops on the structural

315 transect TMTW and additional TMT3 outcrops (Figs 2c, 9). Mapping of these faults along
316 strike reveal an arcuate trend that appears to match the proposed curved nature of the
317 'lobe' / promontory of stacked intrusive sheets (Morgan et al., 2008; Wetmore et al., 2010)
318 emanating from the main intrusion (Fig. 9). There is a distinct lack of Phase 2B faults in the
319 vicinity of transect TMTE. We believe this may be due to the style of emplacement in this
320 area.

321

322 *5.3. Deformation structures at the intrusion contact*

323 Deformation microstructures within the sheared upper contact of the intrusion show brittle
324 to brittle-ductile deformation structures (Figs 10, 11). At the tip and frontal edge of the
325 intrusion contact, sub-vertical fractures and shear bands (with down-to-the-NW kinematics)
326 may be seen (Fig. 10a, d). Similar to those observed at outcrop, stepped intrusion
327 geometries are observed at the micro scale, with steps appearing to be associated with sub-
328 vertical shear-fractures within the host rock (Fig. 10a). These fractures do not appear to
329 extend into the intrusion and are therefore likely to be linked to the emplacement of the
330 magma. Furthermore, magma can also be seen exploiting these sub-vertical shear-fractures
331 (Fig. 10b).

332

333 Further deformation structures can be found on the top surface of the intrusion. Where the
334 contact between intrusive sheets and the host rock can be observed, three distinct layers
335 can be defined (Fig. 10): (1) a 5–10 cm thick baked sandstone layer; (2) a <1 cm thick chilled
336 intrusion margin; and (3) a 1–2 cm zone of aligned (NW–SE) stretched plagioclase
337 phenocrysts (beneath this zone mineral alignment decreases significantly). Low-angle

fracture planes bisect the baked sandstone horizon (Fig. 11a) but do not appear to extend into the intrusion (detaching at the contact?). These fracture planes trend parallel to the intrusion margin (NE–SW), and dip shallowly (~20^{o}) to the SE (Fig. 11a). Slickenlines are preserved on the shear planes in the baked sandstone horizon of the intrusion-host rock contact, showing down-to-the-SE kinematics.

These structures are interpreted to be Riedel shear (R1) fractures consistent with a top-to-the-SE shear sense. Microstructural analysis of the stretched feldspar phenocrysts on the top surface of the intrusive sill sheets (Fig. 11b) indicates significant brittle deformation with shearing of the phenocrysts along multiple fracture planes (Fig. 11c). Kinematics of these fracture planes are also consistent with Riedel shear fractures associated with top-to-the-SE (140^{o}) shear (Fig. 11d).

6. **Kinematics**

Kinematic indicators on Phase 2B dip-slip faults are clearly identifiable as offsets on bedding planes, and steps on slickenlines preserved on the fault surfaces (Figs 4g, 6, 9). The dip-slip faults have both normal and reverse kinematics, with a predominant down-to-the-NW movement, consistent with an overall NW–SE extension or flexure across the margin of the intrusion (Fig. 6c–e). Sense of slip on Phase 2A deformation bands mirrors the kinematics of the Phase 2B faults (Fig. 6a, b), although they are distributed more widely across the intrusion margin. Conjugate sets of extensional deformation bands commonly have an inclined acute bisector axis, consistent with either an original moderately inclined σ3 axis dipping towards the NW, or alternatively rotation about a broadly horizontal axis post-

formation. In either case, the Phase2B fault kinematics are consistent with accommodation of down-to-the-NW extension and rotation.

Strain inversion has been carried out following the Minimized Principal Stress Variation method developed by Reches (1987) using MyFault™ software. This method assumes that the stress required to cause fault slip obeys a Coulomb yield criterion. It is considered that this "strain inversion" technique gives a good approximation for the local palaeostress associated with the intrusion, as the finite slip on faults is relatively small and therefore minimal rotation is likely to have occurred (i.e. strain is a good proxy for stress in low strain environments). Figure 9 shows the bulk inversion for all Phase 2B faults (Fig. 9b), as well as each individual structural station where faults were observed (Fig. 9c). However, it should be noted that significant populations of dip-slip faults were only observed at a limited number of locations (TMTW-3, TMT3-3, TMT3-4, Fig. 9). Bulk inversion suggests that the main stress acting on these faults was extensional (i.e. sub-vertical σ1), with NW–SE (margin perpendicular) oriented extension. Inclination of the stress axes also reflects the flexural component of this extension (σ3 = 338/20; σ1 = 160/70), with extension inclined down towards the NW. Comparisons of the strain inversion at individual structural stations highlight distinct local variations. Spatial variation is observed in the orientation of dip-slip faults, and the kinematic inversion of these individual fault populations reveals a change in the local extensional strain along the intrusion margin (extension varying from NW–SE to NNE–SSW; Fig. 9c). Local variations appear to reflect changes in the stress field, mimicking changes in the orientation of the intrusion margin.

7. **Discussion**

7.1. Deformation phases (pre-, syn-, and late-stage emplacement)

The three distinct deformation phases identified on the north-western margin of the Trachyte Mesa intrusion may be directly linked to specific stages in an emplacement model (pre- Phase 1, syn- Phase 2A and 2B, and late-stage- Phase 3 emplacement).

7.1.1. Phase 1 – Pre-emplacement deformation

Phase 1 deformation structures are found throughout the Trachyte Mesa area, including regions that are significantly distal to the intrusion (Figs 7, 8). As Phase 1 structures do not show any significant spatial or geometric affinity to the Trachyte Mesa intrusion, we suggest that these are likely to have developed prior to emplacement. This is also supported by the consistent cross-cutting relationship observed in the field (i.e. Phase 2 overprinting Phase 1).

Phase 1 deformation structures could be attributed to one or more of a number of late Cretaceous to early Tertiary Laramide uplift deformation events (including the San Rafael Swell, Uncompahgre, Monument, Kaibab, Circle Cliffs, and Miners Mountain uplifts) which resulted in the formation of a series of asymmetrical anticlines (Bump and Davis, 2002), prior to the emplacement of the Trachyte Mesa intrusion. Phase 1 deformation structures appear to have a preferred ENE–WSW trend, although regional analysis reveals a wider spread of orientations, which imply a complicated pre-intrusion deformation history, or that early deformation in the sedimentary cover may have been controlled locally by underlying basement trends (Bump and Davis, 2002).

7.1.2. Phase 2 – Syn-emplacement deformation

Strong spatial, geometric and kinematic relationships between the Phase 2 structures and the intrusion margin lead to the interpretation (cf. Morgan et al., 2008) that this deformation is related to the emplacement of the Trachyte Mesa intrusion.

The relative timings of Phase 2 deformation structures may be further defined through their cross-cutting relationships: Phase 2B faults and ladder zones overprint the more widespread 2A deformation bands. We suggest that this is a result of strain localisation within the overburden during vertical inflation of the underlying sill sheet. The observed monoclinal geometry, and distribution and style of deformation, matches closely to mechanical models of steeply dipping forced folds (Withjack et al., 1990; Johnson and Johnson, 2002). As outlined for traverse TMTW (Fig. 7), Phases 2A and 2B deformation appear to alternate as you move across each individual sill sheet termination. We therefore interpret this to indicate that this 2A–2B strain localisation may be related to the emplacement of each individual sheet rather than the overall intrusion.

7.1.3. Phase 3 – Late-stage emplacement deformation

Phase 3 opening 'Mode 1' joints consistently overprint all other structures in the study area. Phase 3 tensile joints are interpreted to represent late-stage emplacement deformation, rather than post-emplacement deformation. The joints are most likely associated with deflation of the host rocks as the magma body beneath cooled, crystallised and contracted. During vertical inflation of the intrusive sill sheets and overall intrusion, vertical stresses are exerted on the overriding strata. Following cessation of magma flow and contraction of the sheets, this stress is removed, and the overriding host rocks relax and tensile joints (relaxation cooling joints) open. This origin for the Phase 3 joints fits with their wide spatial

distribution over the intrusion, in contrast to the Phase 2B faults, which are localised around sill sheet terminations. A late-stage emplacement timing for the formation of the joints, rather than post-emplacement, is supported by the presence of calcite crystals on the joint surface (Fig. 5g) and 'flame-like', fluid escape structures (Fig. 5h) observed on the top surface of some intrusive sheets, suggesting that these joint sets must have developed while hydrothermal fluids associated with the intrusion were still circulating.

7.2. Modes of Emplacement

Davis (1925) first proposed a model for a protolaccolith spreading to its full lateral extent as a thin sheet before vertical inflation. Hunt (1953) proposed two end-member models ("bulldozing" and "two-stage growth") for laccolith emplacement and growth from a central feeder system. In his general description of the emplacement and growth of laccoliths, Corry (1988) clearly favoured a "two stage growth" model (i.e. radial growth to full lateral extent, followed by vertical growth) and stated that there is no reported field evidence for the remnant hinge zones expected for a radial growth model. Koch et al. (1981), Jackson and Pollard (1988, 1990), Kerr and Pollard (1998) and others suggested that the radial extent of the intrusion may be controlled by the effective thickness of the overburden and the elastic properties of the overlying sandstone. However, as discussed by Corry (1988), other factors such as magma viscosity, strain rate and sheet thickness should also be considered. Although the models of Hunt (1953) and Corry (1988) refer to the emplacement and growth of laccoliths, the concepts are just as applicable to a small sill sheet as they are for larger tabular intrusive bodies.

Corry (1988) made predictions on the likely deformation associated with Hunt's (1953) emplacement models, suggesting that deformation associated with a "bulldozing mechanism" (i.e. radial growth of a full thickness intrusive body) will likely be more complex and distributed than in the "two-stage growth" model. As magma "bulldozes" its way through the host rock, it leaves in its wake a series of remnant deformation "hinge zones" that reflect the propagating deformation front. In contrast, with a "two-stage growth" model, most of the deformation is localised within the high-strain hinge zones at the lateral termination. This is because only minor deformation occurs with the initial radial growth of a thin sheet, and more intense strain developing during the secondary inflation / vertical growth stage.

The kinematics and spatial distribution of these deformation structures may therefore be closely related to the mode of emplacement. Thus deformation is either focused in the area around the periphery of an intrusion, and is less pronounced in the roof zone above the intrusion (Corry, 1988), or, as in the classic beam-bending model for a domal intrusion (Pollard and Johnson, 1973; Kerr and Pollard, 1998), tensile deformation is likely to be distributed across the wider roof area due to flexure.

At Trachyte Mesa, our study has demonstrated that the host-rock deformation structures are strongly localised in the region at the lateral margin of the intrusion, an observation that confirms previous studies of others (Koch et al., 1981; Corry, 1988; Morgan et al., 2008). Although thermal alteration and compaction are apparent in host-rock exposures on the roof of the intrusion, brittle deformation structures such as those described herein on the NW margin are not observed above the intrusion. This, and the fact that there is no

evidence for remnant hinge zones formed by an outward propagating intrusion margin, would suggest that Trachyte Mesa is likely to have formed by “two-stage” growth. The term “punched laccolith” (first used by Gilbert, 1877) has been used to describe relatively flat-topped tabular intrusions, a common characteristic of many laccoliths (including Trachyte Mesa; Morgan et al., 2008), which have formed through two-stage growth. Corry (1988) suggested that deformation / accommodation structures associated with a “bulldozing mechanism” for emplacement are likely to be compression-dominated. In contrast, extension-dominated deformation and accommodation structures are predicted to occur with a “two-stage” / incremental vertical growth mechanism. As all of the emplacement-related deformation structures observed in this study reflect overall extensional strain, our model for emplacement clearly favours the “two-stage” emplacement mechanism.

Morgan et al. (2008) proposed an incremental growth model for the Trachyte Mesa intrusion, through vertical and horizontal growth by the accumulation of multiple horizontal magma sheets. Their emplacement model has strong similarities to the hybrid case of Corry (1988), as both include vertical stacking and lateral sheet propagation (and an outward propagating hinge). In their model, a series of stacked sill sheets are emplaced, with newer sheets emplaced on top of older. This vertical stacking leads to uplift and monoclinal bending of the overlying sandstone units, while in front of the sill sheet terminations a low-pressure triangular-shaped zone develops. Key to the development of this low-pressure zone is the contrasting rock properties of the thinly bedded shaley units (i.e. more deformable) along which the sills are emplaced, and the mechanically strong (and more resistant to bending) overlying massive sandstones (e.g. Fig. 2d). It was envisaged that tongue-like magma sheets would then fill this low-pressure zone, with this process

503 subsequently leading to lateral propagation of the intrusion (and also the outward
504 propagation of a deformation hinge).
505
506 The observations presented here are consistent with an incremental, “stacked sill sheet”
507 growth model for the overall intrusion (cf. Morgan et al., 2008). However, in contrast to that
508 interpretation, evidence for a “two stage” incremental growth mechanism is observed for
509 the emplacement of individual sheets. Furthermore, although contrasting styles of
510 deformation may be observed in the shaley and more massive red sandstone host rock
511 units, no strong evidence exists for incremental lateral sill propagation. Instead we envisage
512 that individual sill sheets were emplaced close to their full radial extent as thin sheets that
513 then vertically inflated through additional magma influx.
514
515 *7.3. Emplacement and structural evolution*
516 Based on the work of previous authors (Corry, 1988; Morgan et al., 2008; Thompson and
517 Schofield, 2008) and our new field observations of intrusion geometries and deformation
518 structures on the NW margin, a new multistage model for the emplacement of Trachyte
519 Mesa intrusion is proposed. This emplacement model is shown in Fig. 12 and discussed in
520 the following sections.
521
522 *7.3.1. Stage 1 - Onset of sheet emplacement and radial growth of a thin “proto-sill”*
523 *sheet*
524 A magma feeder system propagated vertically through the sedimentary pile until it reached
525 a suitable interval for a horizontal sheet to propagate laterally. In the case of Trachyte Mesa
526 this is a thin, mechanically weak, reddish-brown silty sandstone and shale layer occurring

527 between thicker, massive sandstone units (Fig. 5b; Morgan et al., 2008). The “proto-sill”
528 propagated as a thin sheet, with minor inflation, to its maximum lateral extent (Fig. 12). In
529 contrast, Morgan et al. (2008) suggested that lateral sill propagation and thickening may
530 have been episodic [i.e. similar to the hydrid model of Hunt (1953) and Corry (1988)].
531 However, the lack of observable remnant deformation hinge zones on the roof of the
532 intrusion (and others like it; Corry, 1988) favours propagation of a thin proto-sill sheet
533 rather than one with significant inflation. The lateral extent of the sill was likely governed by
534 viscosity of the magma and the properties of the host rock (Thompson and Schofield, 2008).
535
536 Deformation associated with this early emplacement is likely to have been minor, and
537 dominated by shear at the proto-sill sheet contacts (e.g. stretched plagioclase feldspars; Fig.
538 11). As magma flowed in a NE direction, spreading out radially to the NW and SE, shear
539 zones were set up on the top and base surfaces of the intrusion and its contact with the
540 surrounding host rock. These shear structures are likely to show both brittle and plastic
541 deformation characteristics due to the effects of hot magma being emplaced into a cold
542 host rock. Vergence on these shear structures will be opposite to the flow direction of the
543 magma sheet (i.e. on the NW margin, top-to-the-SE-verging shear fabrics occur on the top
544 surface of the intrusion). These shear fabrics may be seen both at outcrop and in thin
545 section (Fig. 11), and have also been defined by AMS (Anisotropy of Magnetic Susceptibility)
546 studies (Morgan et al., 2008). Shear at the intrusion margin is likely to be the first
547 accommodating structure related to the onset of sheet emplacement.
548
549 *7.3.2. Stage 2 - Vertical inflation of sill sheet*

Once the magma had reached its maximum radial extent, vertical inflation commenced as magma supply continued. The thickness of the sill will be governed by the thickness of the overburden (i.e. lithostatic pressure) and the magma pressure (Corry, 1988; Thompson and Schofield, 2008). Thickening of the sill sheet resulted in roof uplift and deformation (e.g. forced folding and fracturing) of the overlying strata This is manifest as conjugate sets of extensional cataclastic deformation band structures (Phase 2A; Figs 4–6), formed in the overlying massive sandstone beds, localised to the developing lateral margin, increasing in intensity around the monoclinal flank above the sill termination (Figs 7, 8, 12).

Although lateral propagation of the sill is likely to have ceased during this inflation phase of emplacement, shear structures still continued to develop on the top surface of the intrusion as magma flowed along the sill. In order to accommodate the additional volume of magma, shear strain on the top surface will have become more dominated by flattening (vertical shortening).

As vertical inflation continued strain became localised at the sill sheet termination resulting in the formation of Phase 2B structures (Figs 6, 12). This strain localisation led to the development of: first, steep deformation corridors cross-cutting earlier conjugate deformation bands (Fig. 6c); and second, the development of principal slip surfaces and ultimately dip-slip faults (Figs 6, 9, 12). These Phase 2B dip-slip faults observed at Trachyte Mesa therefore played a significant role in accommodating the extra volume of magma within the crust.

In the emplacement model of Morgan et al. (2008), sill sheets intruded along a thinly bedded muddy red sandstone and shale unit as full thickness (~1-5 m thickness) tongue-shaped sheets with “bulbous” terminations. A temporary zone of low-pressure was created in front of the intrusion margin as the angle between the stronger massive red sandstone and the weaker silty sandstone and shale unit beneath increased during vertical growth of the intrusion through the accumulation of stacked sheets. In this scenario, magma pressure exceeds lithostatic load, and tongue-like sheets, fed from the stacked sheets, fill the zone of low-pressure, continuing lateral propagation of the intrusion. However, this explanation is inconsistent with the structural evidence, as a zone of low-pressure is unlikely to develop where normal faults accommodate the strain. Instead, it is suggested here that the smooth, curved nature of the “bulbous” sill sheet terminations (Fig. 3a) are the result of inflation (akin to that of the rounded surface of a balloon; Fig. 12a). Had this rounded geometry formed during the sill propagation, there should be more evidence for magma infiltrating the host rock in front of the intrusion, rather than the presence of sheared, steeply-dipping, shaley red sandstone.

7.3.3. Stage 3 - Emplacement of additional sill sheets

Successive sheets were emplaced through the same two-stage emplacement (i.e. radial followed by vertical growth) as for the first sill sheet. Along structural transect TMTW (Fig. 7), the sequence of sill sheet stacking largely appears to have occurred from the bottom of the intrusion upwards, as each successive sill sheet was emplaced on top of the underlying sheet, and hence creating a ‘Christmas-tree’-type laccolith. However, the sequence and level at which successive sheets were emplaced varies significantly (the impact of out-of-sequence stacking is discussed below).

7.3.4. Stage 4 - Onset of sill-climbing

Following the formation of Phase 2B faults during the vertical inflation stage, magma was able to utilise these faults and sill-climbing commenced (Figs 12, 13; Thompson and Schofield, 2008). If the fault plane was able to open, magma was able to propagate along the fault (Figs 3b, 12, 13). At Trachyte Mesa, examples of sill climbing can be observed at both outcrop (Fig. 3b) and in thin section (Fig. 10b). This sill climbing preferentially exploited reverse dip-slip faults (Figs 3b, 13). There are two likely reasons for the magma preferentially exploiting these faults. The first is that the geometry of the reverse faults, dipping towards the sill termination, allowed the magma to continue its outward radial flow up along the fault plane and up through the host stratigraphy. However, probably the most important factor controlling sill climbing along these faults is the stresses induced on the fault due to roof uplift (Fig. 13). If the Phase 2B faults have a normal geometry (i.e. dipping away from the sill sheet), compressional forces, due to both uplifting of the roof strata and loading of the overburden, keep the plane closed and prevent migration of magma along its path (Fig. 13). In contrast, if the fault has a reverse geometry (i.e. dipping towards the sill sheet), roof uplift forces reduce the vertical stress on the fault, thus enabling magma to exploit the fault plane (Fig. 13).

7.3.5. Stage 5 - Cooling and relaxation of intrusion

As the intrusive sheets (and overall intrusive body) started to cool and contract with the cessation of magma flow, the host rocks above also relaxed. During this relaxation of the overriding strata, and the removal of the vertical compressive stresses that had been

620 exerted on the overlying sediments during vertical inflation of the intrusive sheets, tensile
621 joints formed and opened, allowing hydrothermal fluids to circulate (Figs 5g, h, 12).
622
623 *7.4. Sequence of stacking*
624 The sequence in which intrusive sill sheets are stacked plays a significant role in the resulting
625 geometry of the intrusion and the overlying stratigraphy, as well as the types of
626 deformation structures observed in the host rocks. In the two structural transects carried
627 out here (Figs 2, 7, 8), two contrasting styles of intrusion geometry are observed that appear
628 to be the result of different orders of sill stacking. In TMTW, the margin of the intrusion is
629 characterised by a series of sub-horizontal sill sheets of varying thickness (1.5 m) stacked
630 one on top of the other (Fig. 7). This conventional stacking sequence would be consistent
631 with the order of stacking discussed above and outlined in Fig. 12a. In contrast, in TMTE the
632 order of sill stacking appears out-of-sequence. As discussed by Morgan et al. (2008) and
633 highlighted in Fig. 8b, it appears that the lower sub-horizontal sheets were actually
634 emplaced later than upper sheets. The main evidence for this out-of-sequence stacking is
635 the fact that the upper sill sheets have been arched and rotated upwards in a similar
636 monoclinal geometry to the overlying sandstone beds due to the emplacement of sub-
637 horizontal sheets beneath.
638
639 Not only does the sequence of stacking affect the geometry of the intrusion, it also has a
640 significant impact on the style of deformation occurring in the overriding host rock
641 (compare Figs 7, 8). In a sequentially stacked sequence (e.g. TMTW; Fig. 7) a “stepped”
642 bedding profile is developed (i.e. terraces associated with individual sill sheets), and dip-slip
643 faults (Phase 2B) occur at the tips of successive intrusive sheets. In areas where out-of-

644 sequence emplacement is apparent (e.g. TMTE; Fig. 8), the intrusion margin is distinctly
645 monoclinal (i.e. one single step), and due to the presence of the overriding sill sheets,
646 development of Phase 2B faults is inhibited (Fig. 12b). Close to the intrusion contact,
647 compressional deformation structures including small reverse faults are observed, although
648 in the more competent sandstone beds extension-dominated deformation structures still
649 prevail (Fig. 5b).
650
651 *7.5. Faulting at sill terminations*
652 A significant observation from this study, previously undocumented at Trachyte Mesa, is the
653 presence of dip-slip faults associated with individual sill terminations (i.e. Phase 2B
654 structures). Thompson and Schofield (2008) suggested that the main control on the
655 development of faults at sill sheets terminations is the depth of formation. At shallower
656 depths, cohesive strength along bedding planes is less, and so favours the development of
657 flexural slip folding. As depth increases, higher shear stresses are required for flexural slip,
658 thus favouring mechanical failure of the rock through fracture / faulting (Stearns, 1978).
659
660 Pollard and Johnson (1973) presented a conceptual model for the formation of peripheral
661 dykes located at the tips of laccolith bodies from field observations. It was suggested that
662 the dykes formed at the periphery of the intrusions as a result of flexural / elastic bending of
663 the overburden layers (contractional over the centre and extensional over the periphery).
664 Evidence for sill-climbing at Trachyte Mesa is in agreement with such extensional strain at
665 the periphery. However, instead of the strain being accommodated by simple opening
666 'Mode 1' joints, it is proposed that it was the Phase 2B faults that were exploited by the
667 magma (Fig. 3b).

668

669 Sill climbing associated with the exploitation of periphery faults is likely to play a significant
670 role in the development of saucer-shaped sills (Galland et al., 2009; Fig. 13). Thompson and
671 Schofield (2008) took this process a stage further, with the flow pathway of the magma
672 flattening again at some point along the fault plane. This stage has not been observed in
673 exposures at Trachyte Mesa.

674

675 *7.6. Micro-Macro emplacement structures*

676 Intrusions and their associated deformation are typically scalar-invariant in nature
677 (McCaffrey and Petford, 1997). Although it has not been a major focus of this study, it is
678 worthy of note that multiple examples of similar deformation structures occur at both the
679 outcrop and microstructural scales. Examples of this include the steeply dipping, Phase 2b
680 dip-slip faults and shear planes at the tips of intrusive sheets (Figs. 6d, e, 10), propagation of
681 magma along faults (Figs 5h, 10b), Riedel shears associated with shearing on the top surface
682 of the intrusion (Fig. 11), as well as the consistent two-stage growth mechanism for both
683 individual sheets and the entire intrusion. The structural similarities we observe at multiple
684 scales (i.e. thin section, individual intrusive sheets and the overall intrusion) may reflect a
685 scale-invariance which may make our models applicable to larger-scale intrusions (i.e.
686 laccoliths and plutons; cf. Rocchi et al., 2002).

687

688 **8. Conclusions**

689 Trachyte Mesa intrusion, the most distal satellite intrusion of the Mount Hillers intrusive
690 complex in the Henry Mountains Utah, comprises a series of stacked sill sheets.
691 Deformation structures (geometry, kinematics, spatial distribution) associated with the

692 emplacement of the intrusion vary in style and intensity along the intrusion margin. Detailed
693 analysis of the host rock deformation structures and their cross-cutting relationships
694 enables the recognition of three distinct phases, interpreted to represent pre- (Phase 1),
695 syn- (Phase 2), and late-stage (Phase 3) emplacement deformation stages. Spatial and
696 kinematic association of Phase 2 structures (deformation bands and dip-slip faults) indicate
697 extensional strain normal to the intrusion margin during emplacement, with the inclination
698 of the sigma-3 axis reflecting the flexural nature of the margin.
699
700 The preferred emplacement model of a series of stacked sill sheets is in agreement with
701 previous studies (Morgan et al., 2008), but a different mechanism for the emplacement of
702 individual sill sheets is envisaged in which dip-slip faults accommodate sill inflation / vertical
703 growth. All emplacement-related deformation structures observed reflect extensional
704 strain-dominated deformation. Each individual sill sheet is believed to have grown to its
705 maximum radial extent as a thin sheet, and then in a second stage, to inflate vertically to its
706 present thickness. It is likely that most deformation of the host rock took place during this
707 second stage, with faults developing at the sill terminations due to strain localisation.
708
709 Magma preferentially exploited the faults that developed at the periphery of sill sheets,
710 initiating sill climbing. Extensional roof faulting and sill climbing support a two-stage growth
711 history for the overall intrusion. These observations are consistent with theoretical models
712 of sill emplacement (e.g. Pollard and Johnson, 1973; Koch et al., 1981; Thompson and
713 Schofield, 2008).
714

The order in which sill sheets are stacked has impacted the intrusion geometry and associated deformation. In conventionally stacked sequences (i.e. base upwards) a "stepped" / terraced bedding profile develops, with the presence of dip-slip faults localised at the tips of successive intrusive sheets. By contrast, where intrusive sheets are emplaced beneath earlier intruded sheets (i.e. out-of-sequence stacking), the resulting intrusion and host rock geometries and emplacement-related deformation structures are significantly different, having a monoclinal rather than stepped profile, with no dip-slip faults at sill terminations.

Not only do the deformation structures record the strain evolution, and thus mode of emplacement of the intrusion, they also controlled the subsequent propagation of the intrusive body (e.g. in the form of sill climbing). These observations provide new insights on the emplacement mechanisms of sills and laccoliths, how magma is accommodated in the subsurface and how emplacement of high level intrusions can affect sedimentary host rocks.

References

Aydin, A., 1978. Small faults formed as deformation bands in sandstone. Pure and Applied Geophysics, 116, 913–930.

Aydin, A. and Johnson, A.M., 1978. Development of faults as zones of deformation bands and as slip surfaces in sandstones. Pure and Applied Geophysics, 116, 931–942.

Aydin, A. and Johnson, A.M., 1983. Analysis of faulting in porous sandstones. Journal of Structural Geology, 5, 19–31.

737 Bump, A.P. and Davis, G.H., 2003. Late Cretaceous – early Tertiary Laramide deformation of
738 the northern Colorado Plateau, Utah and Colorado. Journal of Structural Geology, 25, 421–
739 440.

740 Coleman, D.S., Gray, W. and Glazner, A.F., 2004. Rethinking the emplacement and evolution
741 of zoned plutons: geochronologic evidence for incremental assembly of the Tuolumne
742 Intrusive Suite, California. Geology, 32, 433–436.

743 Corry, C.E., 1988. Laccoliths: Mechanics of Emplacement and Growth. Geological Society of
744 America, Special Papers, 220, 110 pp.

745 Cruden, A.R and McCaffrey, K.J.W., 2001. Growth of plutons by floor subsidence:
746 implications for rates of emplacement, intrusion spacing and melt-extraction mechanisms.
747 Physics and Chemistry of the Earth Part A: Solid Earth & Geodesy, 26, 303–315.

748 Davis, G.H., 1978. Monocline fold pattern of the Colorado Plateau. In: Matthews, V.I. (Ed.),
749 Laramide Folding Associated with Basement Block Faulting in the Western United States.
750 Geological Society of America Memoir, 151, pp. 215–233.

751 Davis, W.M., 1925. Laccoliths and sills (abs.). Washington Academy of Science Journal, 15,
752 414–415.

753 Davis, G., 1999. Structural geology of the Colorado Plateau region of southern Utah, with
754 special emphasis on deformation bands. Geological Society of America, Special Papers, 342.

755 Du Toit, A.L., 1920. The Karoo dolerites of South Africa: a study in hypabyssal injection.
756 Transactions of the Geological Society of South Africa, 23, 1–42.

757 Engel. C.G., 1959. Igneous rocks and constituent hornblendes of the Henry Mountains, Utah.
758 Geological Society of America Bulletin, 70, 951-980. DOI: 10.1130/0016-
759 7606(1959)70[951:IRACHO]2.0.CO;2.

760 Fossen, H., Schultz, R.A., Shipton, Z.K. and Mair, K., 2007. Deformation bands in sandstone: a
761 review. Journal of the Geological Society London, 164, 755–769. DOI: 10:1144/0016-
762 76492006-36.

763 Galland, O., Planke, S., Neumann, E.-R. and Malthe-Sørenssen, A., 2009. Experimental
764 modelling of shallow magma emplacement: application to saucer-shaped intrusions. Earth
765 and Planetary Sciences Letters, 277, 373–383. DOI: 10.1016/j.epsl.2008.11.003

766 Gilbert, G.K., 1877. Geology of the Henry Mountains, Utah. U.S. Geographical and Geological
767 Survey of the Rocky Mountain Region, 170 pp.

768 Gilbert, G.K., 1896. Laccolites in southeastern Colorado. Journal of Geology, 4, 816–825.

769 Glazner, A.F., Bartley, J.M., Coleman, D.S., Gray, W. and Tayler, R.Z., 2004. Are plutons
770 assembled over millions of years by amalgamation from small magma chambers? GSA
771 Today, 14. doi: 10.1130/1052-5173(2004)013!0004:APAOMOO.

772 Habert, G. and de Saint-Blanquat, M., 2004. Rate of construction of the Black Mesa
773 bysmalith, Henry Mountains, Utah, USA. In: Breitkreutz, C. and Petford, N. (eds.) Physical
774 geology of high-level magmatic systems. Geological Society, London, Special Publication,
775 234, 143–159.

776 Horsman, E., Tikoff, B. and Morgan, S., 2005. Emplacement related fabric in a sill and
777 multiple sheets in the Maiden Creek sill, Henry Mountains, Utah. Journal of Structural
778 Geology, 27, 1426–1444. doi:10.1016/j.jsg.2005.03.003.

779 Hunt, C.B., 1953. Geology and Geography of the Henry Mountains Region, Utah. U.S.
780 Geological Survey Professional Paper, 228, 234 pp.

781 Hunt, C.B., 1988. Geology of the Henry Mountains, Utah, as recorded in the notebooks of
782 G.K. Gilbert, 1975-1876. Geological Society of America Memoir, 167, 229 pp.

783 Hutton, D.H.W., 1996. The 'space problem' in the emplacement of granite. Episodes, Journal
784 of International Geoscience, 19, no 4, 114–119.

785 Hutton, D.H.W., 1997. Syntectonic granites and the principle of effective stress: a general
786 solution to the space problem? In: Bouchez, J.L., Hutton, D.H.W., and Stephens, W.E., (Eds.),
787 Granite: from segregation of melt to emplacement fabrics. Petrology and Structural
788 Geology, 8, 189–197. DOI: 10.1007/978-94-017-1717-5_12

789 Jackson, S.E., and Pollard, D.D., 1988. The laccolith-stock controversy: New results from the
790 southern Henry Mountains, Utah. Geological Society of America Bulletin, 100, 117–139.
791 doi:10.1130/0016-7606.

792 Jackson, S.E., and Pollard, D.D., 1990. Flexure and faulting of sedimentary host rocks during
793 growth of igneous domes, Henry Mountains, Utah. Journal of Structural Geology, 12, 185–
794 206, doi:10.1016/0191-8141(90)90004-I.

795 Johnson, A.M., and Pollard, D.D., 1973. Mechanics of growth of some laccolithic intrusion in
796 the Henry Mountains, Utah, I: Field observations, Gilbert's model, physical properties and
797 flow of the magma. Tectonophysics, 18, 261–309, doi:10.1016/0040-1951(73)90050-4.

798 Johnson, K.M., and Johnson, A.M., 2002. Mechanical analysis of the geometry of forced-
799 folds. Journal of Structural Geology, 24, 401–410.

800 Kerr, A.D., Pollard, D.D., 1998. Towards more realistic formulations for the analysis of
801 laccoliths. Journal of Structural Geology, 20, 1783–1793.

802 Koch, F.G., Johnson, A.M., and Pollard, D.D., 1981. Monoclinal bending of Strata over
803 laccolithic intrusions. Tectonophysics, 74, T21–T31.

804 Larson M.J, Bromfield C.S., Dubiel R.F., Patterson C.G. and Peterson F., 1985. Geologic map
805 of the Little Rockies wilderness study area and the Mt. Hillers and Mt. Pennell study areas,
806 and vicinity, Garfield County, Utah. U.S. Geological Survey Map MF-1776-B.

807 Magee, C., Stevenson, C. T., O'Driscoll, B. and Petronis, M., 2012. Local and regional controls
808 on the lateral emplacement of the Ben Hiant dolerite intrusion, Ardnamurchan (NW
809 Scotland). Journal of Structural Geology, 39, 66–82. doi.org/10.1016/j.jsg.2012.03.005

810 Mahan, K.H., Bartley, J.M., Coleman, D.S., Glazner, A.F. and Carl, B., 2003. Sheeted intrusion
811 of the synkinematic McDoogle pluton, Sierra Nevada, California. Geological Society of
812 America Bulletin, 115, 1570–1582.McCaffrey, K.J.W. and Petford, N., 1997. Are granitic
813 intrusions scale invariant? Journal of the Geological Society London, 154, 1–4.

814 Petford, N., Cruden, A.R., McCaffrey K.J.W. and Vignerosse, J.L., 2000. Granitic magma
815 formation, transport and emplacement in the Earth's Crust. Nature, 408, 669–673

816 Morgan, S., Horsman, E., Tikoff, B., de Saint Blanquat, M., Nugent, A. and Habert G., 2005.
817 Sheet-like emplacement of satellite laccoliths, sills and bysmaliths of the Henry Mountains,
818 southern Utah. In: Pederson J. and Dehler, C.M. (Eds.), Interior Western United States Field
819 Guide, GSA Field Guides, 6, 283–309. doi: 10.1130/2005.fld006(14)

820 Morgan, S., Stanik, A., Horsman, E., Tikoff, B., de Saint Blanquat, M. and Habert., G., 2008.
821 Emplacement of multiple magma sheets and wall rock deformation: Trachyte Mesa
822 intrusion, Henry Mountains, Utah. Journal of Structural Geology, 30, 491–512,
823 DOI:10.1016/j.jsg.2008.01.005.

824 Nelson, S.T., Davidson, J.P. and Sullivan, K.R., 1992. New age determinations of central
825 Colorado Plateau laccoliths, Utah: Recognizing disturbed K–Ar systematics and re-evaluating
826 tectonomagmatic relationships. Geological Society of America Bulletin, 104, 1547–1560.

827 Nelson, S.T. and Davidson, J.P., 1993. Interactions between mantle-derived magmas and
828 mafic crust, Henry Mountains, Utah. Journal of Geophysical Research B2, 98, 1837–1852.
829 Pitcher, W.S., 1970. Ghost stratigraphy in intrusive granites: a review. In: Newall, G. and
830 Rast, N. Eds.), Mechanism of Igneous Intrusion, Liverpool, Gallery Press, 123–140.
831 Pollard, D.D. and Johnson, A.M., 1973. Mechanics of growth of some laccolithic intrusions in
832 the Henry Mountains, Utah, II: bending and failure of overburden layers and sill formation.
833 Tectonophysics, 18, 261–309.
834 Pollard, D.D., Muller, O.H. and Dockstader, D.R., 1975. The form and growth of fingered
835 sheet intrusions. Geological Society of America Bulletin, 3, 351–363.
836 Pollard, D.D., 1987. Elementary fracture mechanics applied to the structural interpretation
837 of dykes. In: Halls, H.C. and Fahrig, W.F. (Eds.) Mafic Dyke Swarms. Geological Association of
838 Canada, Special Paper, 34, 5–24.
839 Reches, Z., 1987. Determination of the tectonic stress tensor from slip along faults that obey
840 the Coulomb yield condition. Tectonics, 6, 849–861
841 Rocchi, S., Westerman, D.S., Dini, A., Innocenti, F. and Tonarini, S., 2002. Two-stage laccolith
842 growth at Elba Island (Italy). Geology, 30, 983–986.
843 Saint Blanquat, M. (de) and Tikoff, B., 1997. Development of magmatic to solid-state fabrics
844 during syntectonic emplacement of the Mono Creek Granite, Sierra Nevada Batholith. In:
845 Bouchez, J.L., Hutton, D.H.W, Stephens, W.E. (Eds.), Granite: From Segregation of Melt to
846 Emplacement Fabrics. Kluwer Academic Publishers, Dordrecht, 231–252.
847 Saint Blanquat, M. (de), Habert, G., Horsman, E., Morgan, S., Tikoff, B., Launeau, P. and
848 Gleizes, G., 2006. Mechanisms and duration of non-tectonically, assisted magma

849 emplacement in the upper crust: Black Mesa pluton, Henry Mountains, Utah.
850 Tectonophysics, 428, 1–31, doi:10.1016/j.tecto.2006.07.014.

851 Schofield, N., Stevenson, C. and Reston, T., 2010. Magma fingers and host rock fluidization in
852 the emplacement of sills. Geology, 38, 63–66.

853 Schofield, N.J., Brown, D.J., Magee, C. and Stevenson, C.T., 2012. Sill morphology and
854 comparison of brittle and non-brittle emplacement mechanisms. Journal of the Geological
855 Society London, 169, 127–141.

856 Shipton, Z.K. and Cowie, P.A., 2001. Damage zone and slip-surface evolution over μm to km
857 scales in high-porosity Navajo sandstone, Utah. Journal of Structural Geology, 23, 1825–
858 1844.

859 Stevenson, C.T.E., Owens, W.H., Hutton, D.H.W., Hood, D.N. and Meighan, I., 2007a.
860 Laccolithic, as opposed to cauldron subsidence, emplacement of the Eastern Mourne
861 pluton: Evidence from anisotropy of magnetic susceptibility: Journal of Geological Society
862 London, 164, 99–110. doi: 10.1144/0016076492006-008.

863 Stevenson, C.T.E., Owens, W.H. and Hutton, D.H.W., 2007b. Flow lobes in granite: The
864 determination of magma flow direction in the Trawenagh Bay Granite, north-western
865 Ireland, using anisotropy of magnetic susceptibility. GSA Bulletin, 119, 1368–1386. doi:
866 10.1130/B25970.1

867 Thompson, K., 2004. Sill complex geometry and internal architecture: a 3D seismic
868 perspective. In: Breitkreutz, C. and Petford, N. (eds.) Physical Geology of High-level
869 Magmatic Systems. Geological Society London, Special Publication, 234, 229–232.

870 Thomson, K. and Hutton, D., 2004. Geometry and growth of sill complexes: insights using 3-
871 d seismic from the North Rockall Trough. Bulletin of Volcanology, 66, 364–375.

872 Thompson, K. and Schofield, N., 2008. Lithological and structural controls on the
873 emplacement and morphology of sills in sedimentary basins. In: Thompson, K. and Petford,
874 N. (Eds.) Structure and Emplacement of High-Level Magmatic Systems. Geological Society
875 London, Special Publication, 302, 31–44.

876 Tikoff, B., Blenkinsop, T., Kruckenberg, S.C., Morgan, S., Newman, J. and Wojtal, S., 2013. A
877 perspective on the emergence of modern structural geology: Celebrating the feedbacks
878 between historical-based and process-based approaches. Geological Society of America
879 Special Papers, 500, 65–119. doi: 10.1130/2013.2500(03)

880 Westerman, D.S., Dini, A., Innocenti, F. and Rocchi, S. 2004. Rise and fall of a nested
881 Christmas-tree laccolith complex, Elba Island, Italy. In: Breitkreuz, C. and Petford, N. (Eds.)
882 Physical Geology of High-level Magmatic Systems. Geological Society London, Special
883 Publication, 234, 195–213.

884 Wetmore, P.H., Connor, C.B., Kruse, S.E., Callihan, S., Pignotta, G., Stremtan, C. and Burke A.,
885 2009. Geometry of the Trachyte Mesa intrusion, Henry Mountains, Utah: Implications for
886 the emplacement of small melt volumes into the upper crust. Geochemistry Geophysics
887 Geosystems, 10, Q08006. DOI: 10.1029/2009GC002469.

888 Wilson, P.I.R. and McCaffrey, K.J.W., 2013. Intrusion space problem: digital mapping and
889 analysis of the Maiden Creek satellite intrusion, Henry Mountains Utah. Geoscientist, 23 (6),
890 16–19.

891 Wilson, P.I.R., McCaffrey, K.J.W., and Holdsworth, R.E., In Prep. Syn-emplacement
892 accommodation structures of igneous intrusions: Maiden Creek intrusion, Henry Mountains,
893 Utah. For submission to Geosphere.

894 Withjack, M.O., Olson, J. and Peterson, E., 1990. Experimental models of extensional forced
895 folds. AAPG Bulletin, 74, 1038–1054.

896

Figure Captions

Fig. 1. Simplified geological maps of the study area. (a) The Henry Mountains region (adapted from Morgan et al., 2008) and its location within Utah (inset map). (b) Mount Hillers and its satellite intrusions (modified from Larson et al., 1985). In (b), the various intrusions that comprise the Mt Hillers intrusive complex are numbered, using the names given by Hunt (1953) : 1 – Mt Hillers central complex; 2 – Bulldog Peak intrusion; 3 – Stewart Ridge intrusion; 4 – Specks Ridge intrusion; 5 – Chaparral Hills Laccolith; 6 – Specks Canyon; 7 – speculated feeder system to the Trachyte Mesa intrusion; 8 – Black Mesa intrusion; 9 – Sawtooth Ridge intrusion; 10 - Maiden Creek intrusion; and 11 – Trachyte Mesa intrusion.

Fig. 2. Location of the study sections. (a) Contoured and georeferenced aerial image of the Trachyte Mesa area showing the intrusion outline of Morgan et al. (2008). Locations of structural stations are shown by the blue filled circles. (b) 3D DEM model of the Trachyte Mesa area, view looking NE. Note viewpoint location for photo (e). (c) Contoured and georeferenced aerial image of field study area, located on the southern end of the NW margin of the intrusion. Structural station localities, bedding measurements, structural transect lines (TMTE, TMTW) and detailed study area (TMT3) are shown. (d) Schematic cross-sections (NW–SE) across the Trachyte Mesa intrusion, showing stacked sill sheets (after Morgan et al., 2008). (e) Field photograph showing monoclinal upper contact and stacked intrusive sheets observed at NW margin of intrusion. Note, zoom in image in (d) is based on the field observations at this outcrop locality.

Fig. 3. Photographs and interpretative sketches showing outcrop geometries of stacked sill sheets on the southern NW margin of Trachyte Mesa. (a) View looking SE from station TMTE-6 along structural transect TMTE. (b) View looking NE from station TMTW-2 onto structural transect TMTW (foreground). N.B. Structural transect TMTE can be seen in the background. Key observations to note are: monoclinal geometry of overriding sandstone units, (a) and (b); flexed / monoclinal upper sill sheets (a) vs. sub-horizontal stacked sill sheets (b); sub-horizontal lower sill sheets with "bulbous" terminations (a) and (b); sill climbing in upper sill sheet, propagating along reverse dip-slip fault (b).

Fig. 4. Summary stereoplots of field structural data. Equal area, lower hemisphere stereoplots of data showing poles to planes (contoured) sorted by structural type: (a) bedding, (b) deformation bands, (c) faults, (d) opening 'Mode 1' joints; and structural phase: (e) Phase 1, (f) Phase 2A, (g) Phase 2B, (h) Phase 3. Mean planes for distinct cluster populations are shown for each plot. Plots (c) and (g) also show fault slip lines with movement direction indicated (solid fill = normal fault slip; white fill = reverse slip).

Fig. 5. Annotated field photographs showing examples of Phase 1 (a), Phase 2 (b–d), and Phase 3 (e–h) deformation structures. (a) Background deformation bands cutting the Entrada Sandstone distal to the intrusion (0.2–2m spacing). (b) Deformation structures at intrusion contact, locality TMTE-9 in Fig. 3. Low angle shear and reverse faults (top-to-the-SE) on top surface of the intrusion and within the highly deformed shaley red sandstone layer adjacent to the contact. Extensional conjugate deformation bands in massive red sandstone (also see fig. 9 in Morgan et al., 2008). (c) Closely spaced porosity reducing

deformation bands in massive red sandstone, localised to intrusion margin and host-rock overlying the top surface of the intrusion (0.5–5cm spacing). (d) Dip-slip normal fault (down-to-the-NW) with well-preserved slickenlines on principal slip surface. (e) Opening 'Mode I' joints trending perpendicular to the intrusion margin (NW–SE), 0.5–2m spacing. (f) Opening 'Mode I' joints trending parallel to the intrusion margin (NE–SW), 1–2m spacing. (g) Calcite crystals precipitated on margin parallel joint surfaces in (f). (h) Calcite precipitation and apparent fluid exploitation of joint systems on top surface of intrusion.

Fig. 6. Annotated field photographs showing additional examples of Phase 2A (a–b) and 2B (c–e) structures and kinematics. (a) Monoclinal bedding geometries in sandstone units ~30 m above the intrusion showing conjugate fault / deformation band geometries consistent with flexure (note offset on bedding in paler sandstone unit). (b) Outcrop example (~5 m above intrusion) of conjugate deformation banding showing consistent offsets to those seen in (a). (c) Steep ladder zone (down-to-the-NW shear) overprinting conjugate deformation bands. Note kinematics of background deformation bands and ladder zone are the same. (d) Outcrop example of normal faults developed at the termination of sill sheets. Note, total throw on normal faults is consistent with the thickness of the individual sill sheet, implying that the faults may be induced by sill sheet inflation. (e) Zoomed-in area outlined in (d) showing ~50 cm normal (down-to-the-NW) offset of bedding contact (PSS – Principal Slip Surface; DZ – Damage Zone).

Fig. 7. Structure along Trachyte Mesa transect TMTW. Cross section (for location see Fig. 2c) constructed in 2D Move™. Equal area, lower hemisphere plots of poles to planes highlight

deformation structure populations collected at each station (white stars; bedding planes highlighted in yellow). Note the stepped / terraced geometry of the margin. Colour bars across the lower part of the section show the spatial distribution of the different deformation phases.

Fig. 8. Structure along Trachyte Mesa transect TMTE. (a) Cross section (for location see Fig. 2c) constructed in 2D Move™. See Fig. 7 for key. Note, the main intrusion is in the SE (to the right) of the section, while a smaller distal intrusion fan be seen further outboard. (b) Close-up of the area around the intrusion margin and corresponding field photograph of the same outcrops. Numbers 1–5 indicate the possible timing of sheet emplacement, with 1 being the earliest sheet. Note the monoclinal geometry of the upper sill sheets and overriding massive sandstone.

Fig. 9. Field photographs and structural data demonstrating the arcuate trend of Phase 2B faults. (a), (b) Equal area lower hemisphere stereoplots showing all fault trends of Phase 2B faults. Faults show dip-slip normal and reverse movements, consistent with NW–SE extension (note inclination of sigma-3, associated with flexure along the intrusion margin). (c) Map showing the distribution of the main outcrop localities at which Phase 2B fault data were collected. The change in geometry and kinematics of the faults with the changing trend of the intrusion margin can be seen from the equal area lower hemisphere plots for each outcrop showing poles to planes, slickenlines and interpreted kinematics. Solid white lines depict areas where intrusion margin is exposed in outcrop, dashed white lines show inferred continuation of margin beneath sandstone beds (note, magnetic data from

989 Wetmore et al. (2009) was used to guide this subsurface geometry). (d) – (f) Field
990 photographs showing outcrop examples of Phase 2 dip-slip normal faults. Although
991 individual faults are quite linear, a clear rotation in fault trend may be seen when walking
992 along strike. Many fault surfaces have well-developed slickenlines showing almost pure dip-
993 slip kinematics.

994

995 **Fig. 10.** Photomicrographs of microstructures observed at the intrusion – sandstone contact.
996 (a) Stepped vertical contact at the tip of an intrusive sill sheet. (b) Magma injecting upwards
997 along an extensional fracture. (c) Top surface of intrusion showing sharp contact and narrow
998 altered margin. (d) Sub-vertical fracture within host rock adjacent to contact, showing
999 down-to-the-NW movement. (e) Oriented sample highlighting area of thin section and
1000 location of images (a) – (d).

1001

1002 **Fig. 11.** Flow generated fabrics at the intrusion margin. (a) Outcrop photograph showing
1003 low-angle brittle extensional faults (see inset stereoplot) cutting baked sandstone unit on
1004 top surface of an intrusive sheet. These are interpreted to be equivalent to R1 Riedel shear
1005 planes, depicted in (d). The faults are only apparent in the baked sandstone and appear to
1006 terminate at the intrusion-host rock interface. (b) Stretched plagioclase phenocrysts within
1007 a strongly sub-horizontal foliated zone (2–3 cm) on the top surface of an intrusive sheet.
1008 Note also the thin (<1 cm) chilled margin zone above the stretched phenocryst / foliated
1009 layer. (c) Photomicrograph of deformed, elongate plagioclase phenocryst within the
1010 uppermost 2–3cm of an intrusive sheet (note section is cut along a vertical plane oriented
1011 parallel to the stretching direction, 140°–320°). The phenocryst is deformed mainly by brittle

1012 deformation and a series of preferred deformation planes, with offset, can be identified.
1013 The movement and orientation of these planes are consistent with Riedel fractures
1014 associated with top-to-the-right (SE) sub-horizontal shear. (d) Schematic cartoon depicting
1015 the deformation structures observed at outcrop and in thin section on the top surface of an
1016 intrusive sheet. The structures and kinematics are consistent with top-to-the-SE sub-
1017 horizontal shear. This shearing is likely driven by magmatic flow within the underlying sheet,
1018 leading to sub-horizontal shortening and shear at the intrusion contact.

1019

1020 **Fig. 12.** Schematic diagram outlining a two-stage growth model for sill emplacement at the
1021 Trachyte Mesa intrusion and associated deformation structures. (a) Conventional stacking
1022 model (as observed at TMTW study area; Fig. 7). Stages of emplacement, as discussed in
1023 text, are: Stage 1 - Sill initiation and radial growth as a thin "proto-" sill sheet; Stage 2 -
1024 Thickening of the sill sheet, resulting in roof uplift and strain localisation in the host rock at
1025 the sill sheet termination; Stage 3 - Emplacement of a second sill sheet (repetition of stages
1026 1 and 2 for 2nd sheet); Stage 4 - Sill climbing through the exploitation of faults developed
1027 during Stage 2; Stage 5 – Sill flattening (not observed at Trachyte Mesa) and late stage
1028 cooling and relaxation of the intrusion. (b) Schematic illustration highlighting the impact of
1029 out-of-sequence stacking (equivalent to Stage 2 in (a) on margin geometry and deformation
1030 structures (as observed in TMTE study area; Fig. 8).

1031

1032 **Fig. 13.** Faulting accompanying sill emplacement. (a) Schematic diagram showing the
1033 development of a saucer-shaped sill (after Galland et al., 2009). (b) Development of dip slip

faults at sill tips during two-stage growth model and implications for sill climbing and vertical propagation.

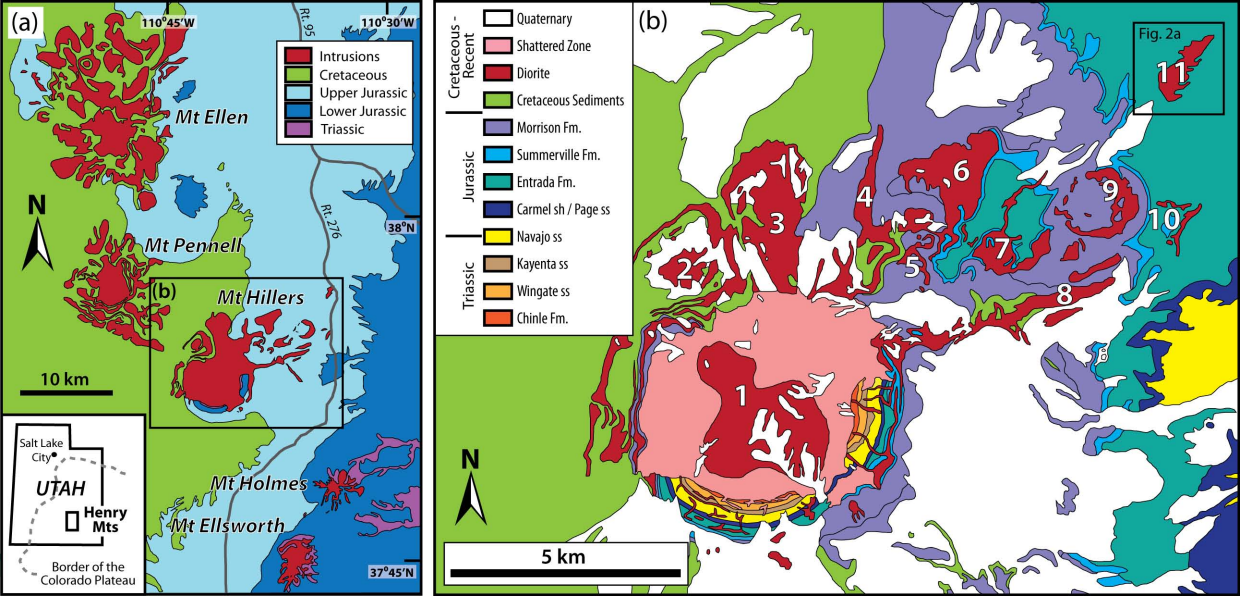
(a)
110°45'W
110°30'W
Rt. 95
Rt. 276
38°N
37°45'N
Intrusions
Cretaceous
Upper Jurassic
Lower Jurassic
Triassic
Mt Ellen
Mt Pennell
Mt Hillers
Mt Holmes
Mt Ellsworth
N
10 km
(b)
Salt Lake City
UTAH
Henry Mts
Border of the Colorado Plateau
Cretaceous - Recent
Jurassic
Triassic
Quaternary
Shattered Zone
Diorite
Cretaceous Sediments
Morrison Fm.
Summerville Fm.
Entrada Fm.
Carmel sh / Page ss
Navajo ss
Kayenta ss
Wingate ss
Chinle Fm.
(b)
Fig. 2a
1
2
3
4
5
6
7
8
9
10
11
N
5 km

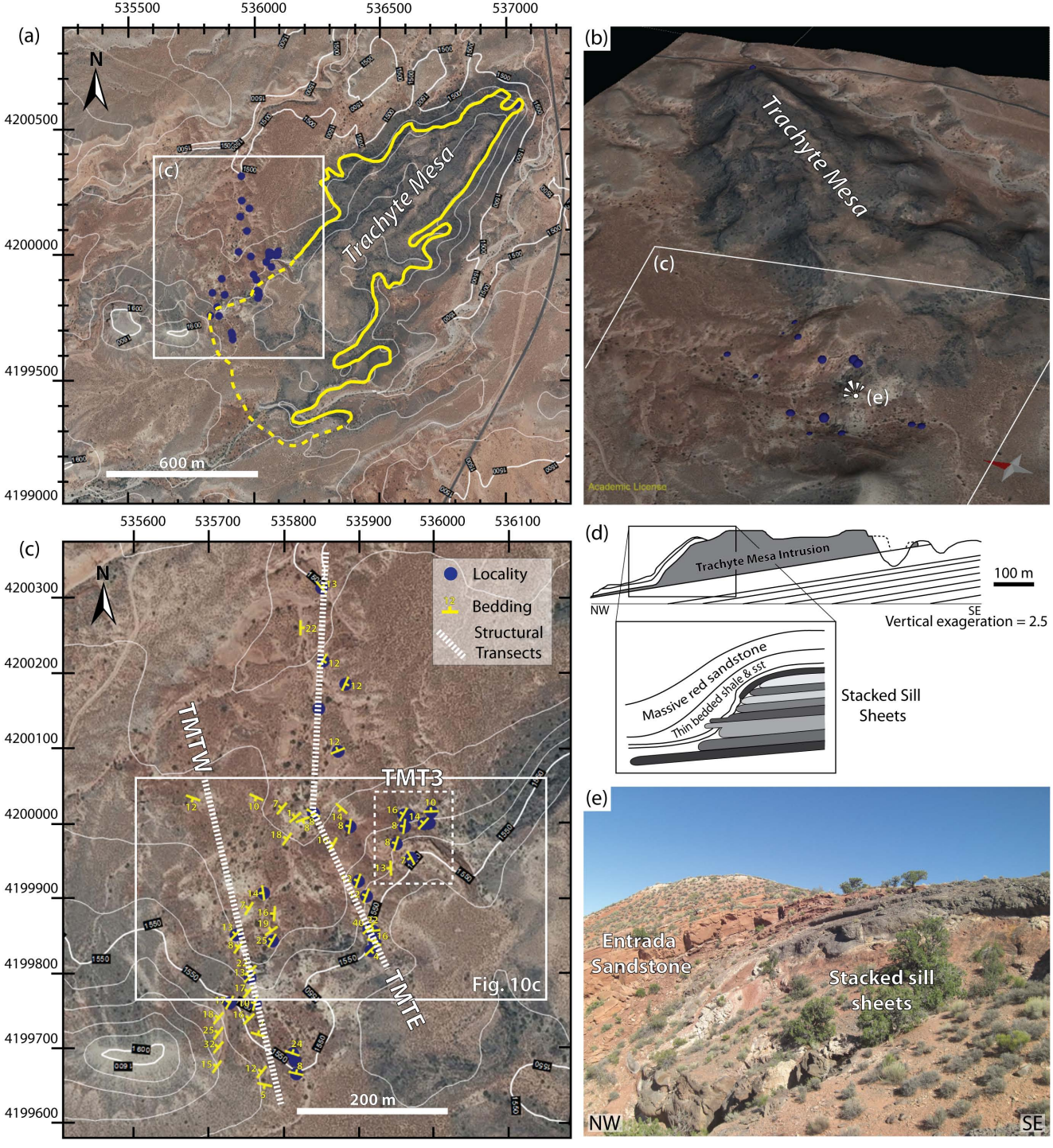
(a)
N
Trachyte Mesa
(c)
600 m
535500
536000
536500
537000
4200500
4200000
4199500
4199000
(b)
Trachyte Mesa
(c)
(e)
Academic License
(c)
N
Locality
Bedding
Structural Transects
TMTW
TMT3
TMTE
Fig. 10c
200 m
535600
535700
535800
535900
536000
536100
4200300
4200200
4200100
4200000
4199900
4199800
4199700
4199600
(d)
Trachyte Mesa Intrusion
100 m
NW
SE
Vertical exageration = 2.5
Massive red sandstone
Thin bedded shale & sst
Stacked Sill Sheets
(e)
Entrada Sandstone
Stacked sill sheets
NW
SE

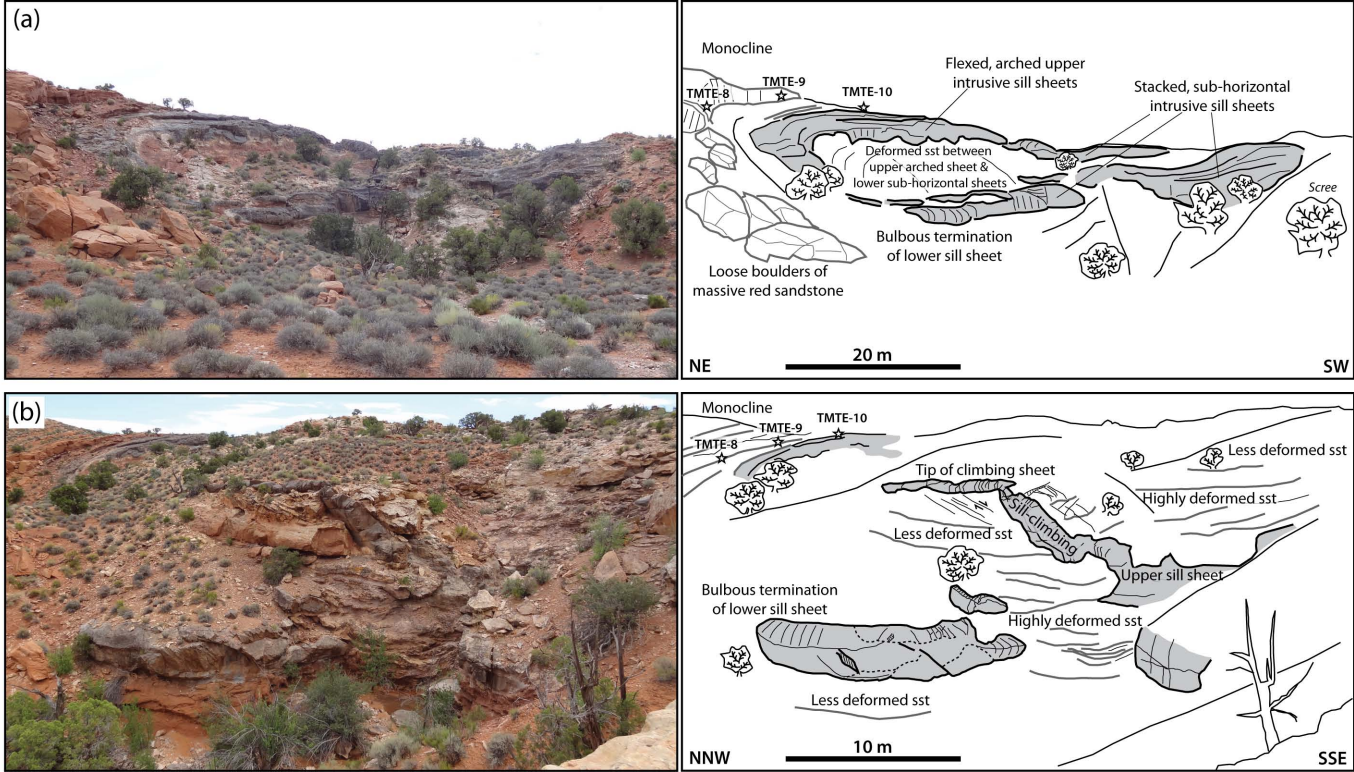
(a)
Monocline
TMTE-8
TMTE-9
TMTE-10
Flexed, arched upper intrusive sill sheets
Stacked, sub-horizontal intrusive sill sheets
Deformed sst between upper arched sheet & lower sub-horizontal sheets
Scree
Bulbous termination of lower sill sheet
Loose boulders of massive red sandstone
NE
20 m
SW
(b)
Monocline
TMTE-8
TMTE-9
TMTE-10
Tip of climbing sheet
Less deformed sst
Highly deformed sst
Sill climbing
Less deformed sst
Upper sill sheet
Bulbous termination of lower sill sheet
Highly deformed sst
Less deformed sst
NNW
10 m
SSE

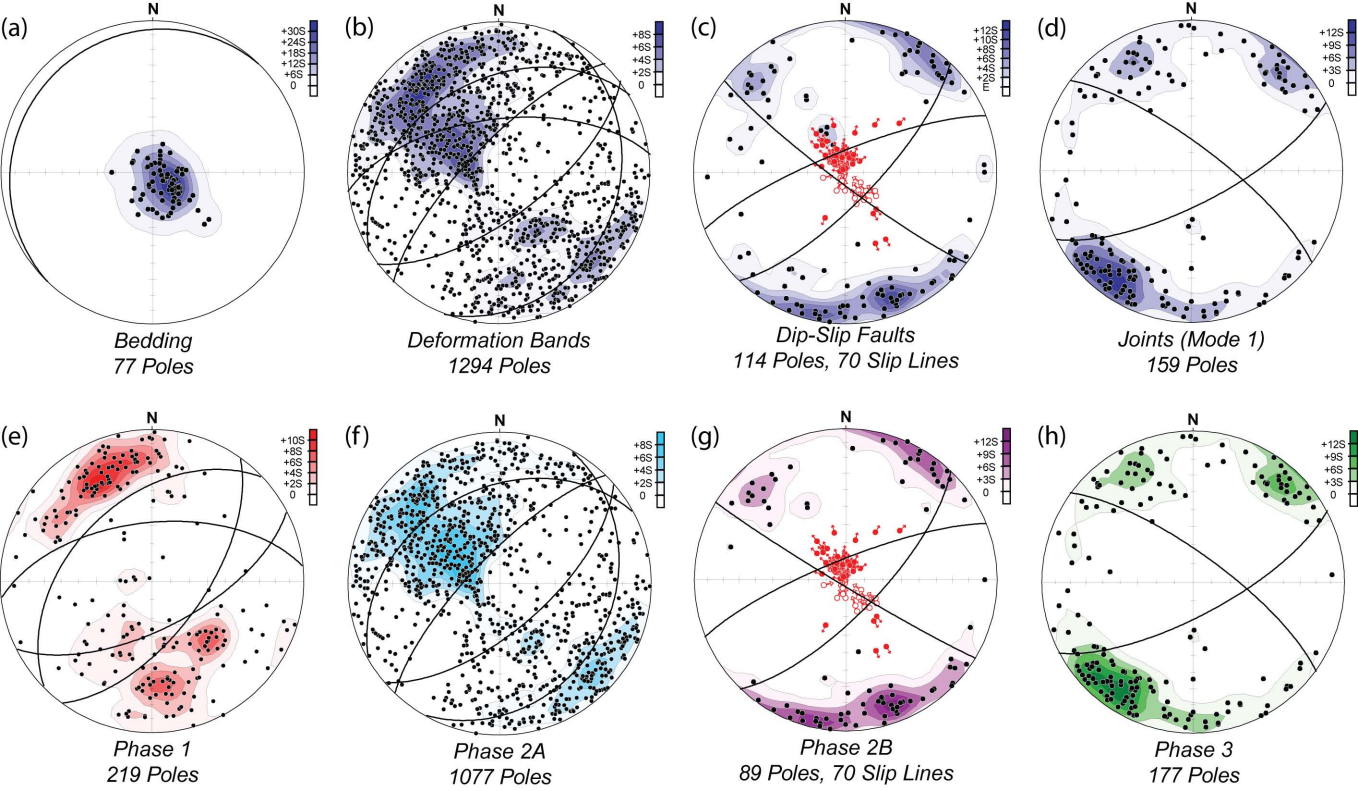
(a)
N
+30S
+24S
+18S
+12S
+6S
0
Bedding
77 Poles
(b)
N
+8S
+6S
+4S
+2S
0
Deformation Bands
1294 Poles
(c)
N
+12S
+10S
+8S
+6S
+4S
+2S
E
Dip-Slip Faults
114 Poles, 70 Slip Lines
(d)
N
+12S
+9S
+6S
+3S
0
Joints (Mode 1)
159 Poles
(e)
N
+10S
+8S
+6S
+4S
+2S
0
Phase 1
219 Poles
(f)
N
+8S
+6S
+4S
+2S
0
Phase 2A
1077 Poles
(g)
N
+12S
+9S
+6S
+3S
0
Phase 2B
89 Poles, 70 Slip Lines
(h)
N
+12S
+9S
+6S
+3S
0
Phase 3
177 Poles


(a)
NW
1 m
SE
(b)
2A Def. Bands
Massive Red Sst
Muddy Red, Shaley Sst
Upper sill sheet
Lower sill sheet
NW
2 m
SE
(c)
NW
SE
(d)
FW
HW
ESE
WNW
(e)
Intrusion
Margin Perpendicular Joints
NE
5 m
SW
(f)
Intrusion
Margin Parallel Joints
NW
10 m
SE
(g)
SW
NE
(h)
SW
NE

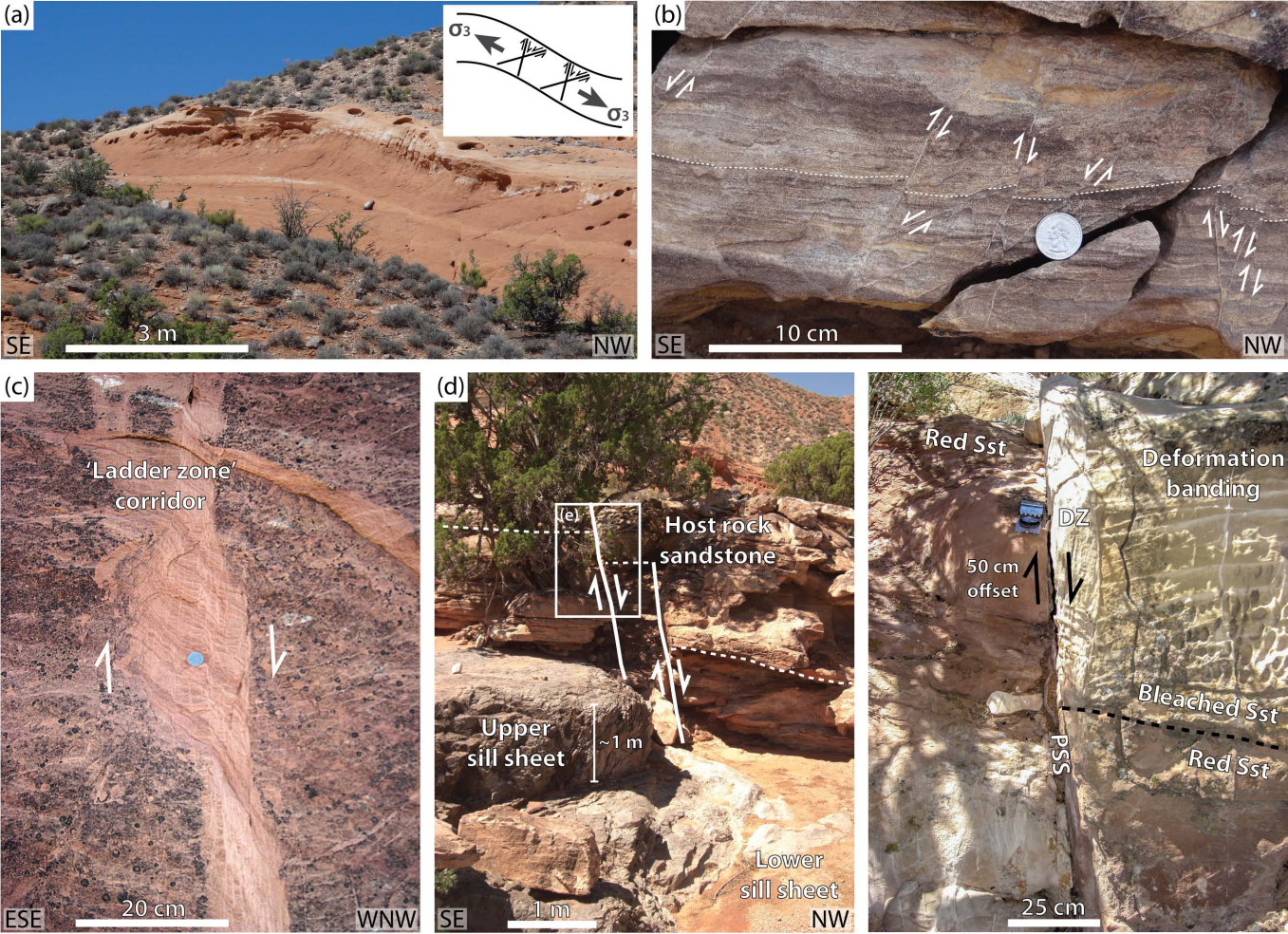
(a)
σ3
σ3
SE
3 m
NW
(b)
SE
10 cm
NW
(c)
'Ladder zone'
corridor
ESE
20 cm
WNW
(d)
(e)
Host rock
sandstone
Upper
sill sheet
~1 m
Lower
sill sheet
SE
1 m
NW
Red Sst
Deformation
banding
DZ
50 cm
offset
Bleached Sst
PSS
Red Sst
25 cm

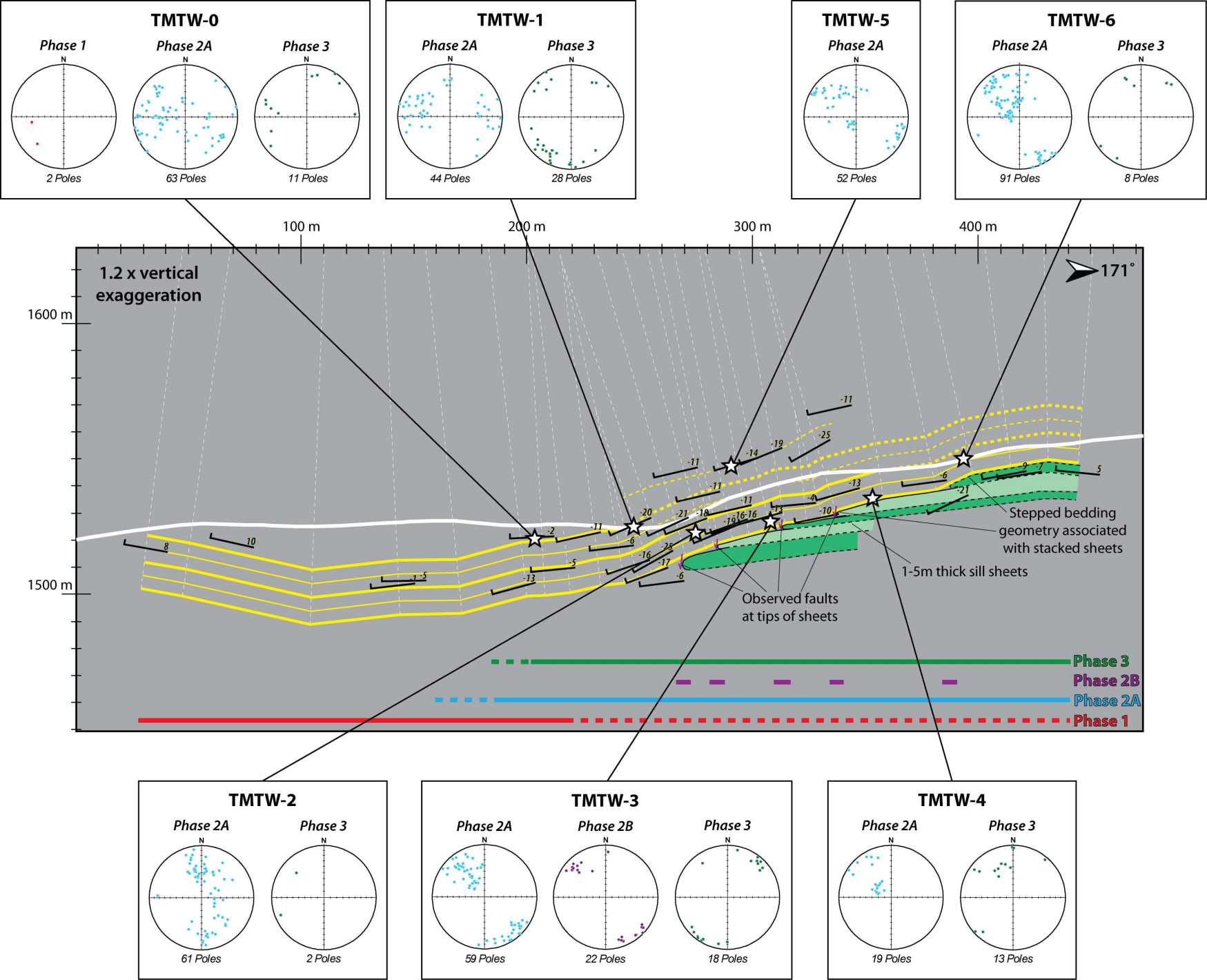
TMTW-0
Phase 1
Phase 2A
Phase 3
2 Poles
63 Poles
11 Poles
TMTW-1
Phase 2A
Phase 3
44 Poles
28 Poles
TMTW-5
Phase 2A
52 Poles
TMTW-6
Phase 2A
Phase 3
91 Poles
8 Poles
100 m
200 m
300 m
400 m
1.2 x vertical exaggeration
171°
1600 m
1500 m
Stepped bedding geometry associated with stacked sheets
1-5m thick sill sheets
Observed faults at tips of sheets
Phase 3
Phase 2B
Phase 2A
Phase 1
TMTW-2
Phase 2A
Phase 3
61 Poles
2 Poles
TMTW-3
Phase 2A
Phase 2B
Phase 3
59 Poles
22 Poles
18 Poles
TMTW-4
Phase 2A
Phase 3
19 Poles
13 Poles

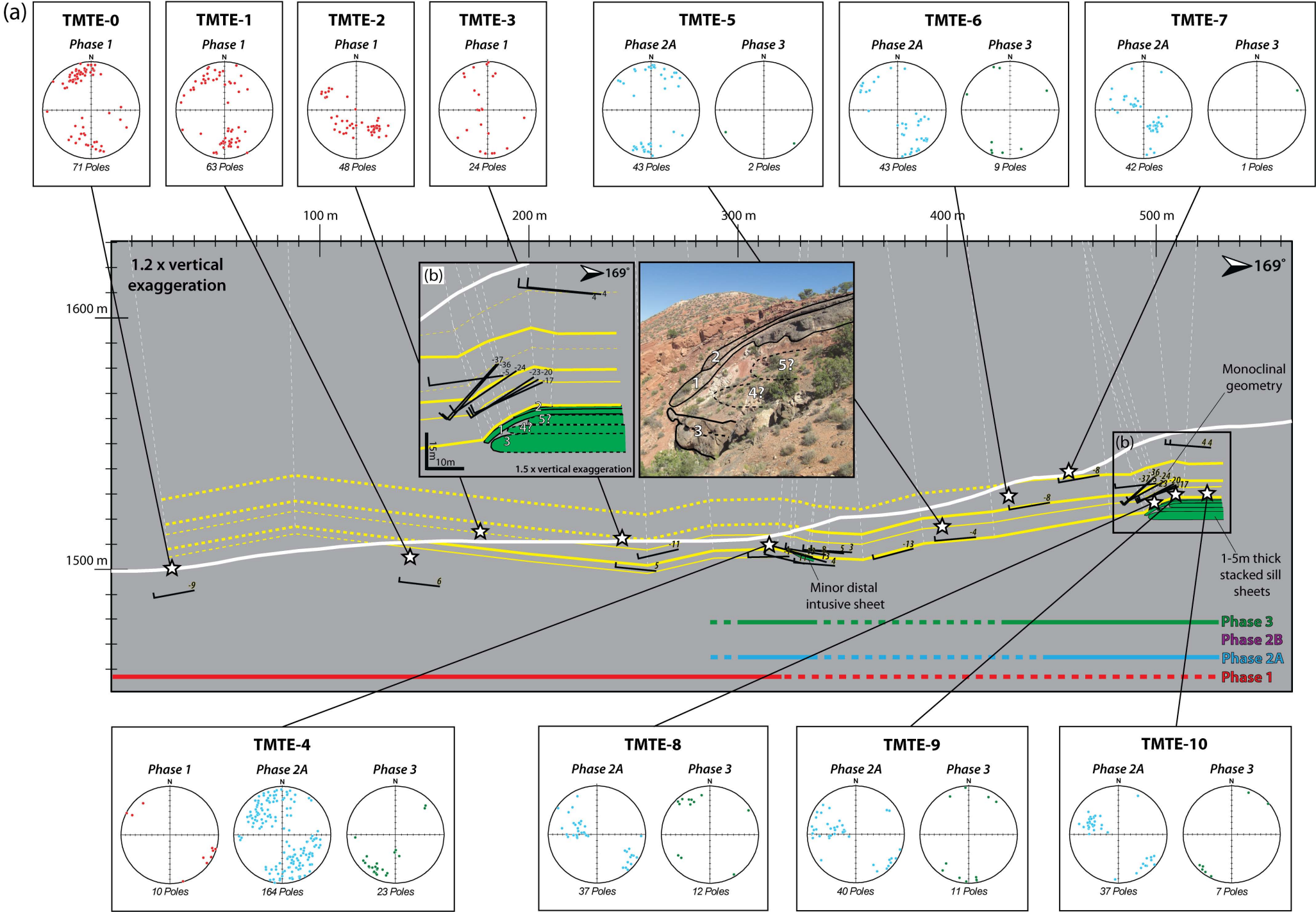
(a)
TMTE-0
Phase 1
71 Poles
TMTE-1
Phase 1
63 Poles
TMTE-2
Phase 1
48 Poles
TMTE-3
Phase 1
24 Poles
TMTE-5
Phase 2A
43 Poles
Phase 3
2 Poles
TMTE-6
Phase 2A
43 Poles
Phase 3
9 Poles
TMTE-7
Phase 2A
42 Poles
Phase 3
1 Poles
100 m
200 m
300 m
400 m
500 m
1.2 x vertical exaggeration
1600 m
1500 m
(b)
169°
1.5m
10m
1.5 x vertical exaggeration
Monoclinal geometry
Minor distal intusive sheet
1-5m thick stacked sill sheets
Phase 3
Phase 2B
Phase 2A
Phase 1
TMTE-4
Phase 1
10 Poles
Phase 2A
164 Poles
Phase 3
23 Poles
TMTE-8
Phase 2A
37 Poles
Phase 3
12 Poles
TMTE-9
Phase 2A
40 Poles
Phase 3
11 Poles
TMTE-10
Phase 2A
37 Poles
Phase 3
7 Poles

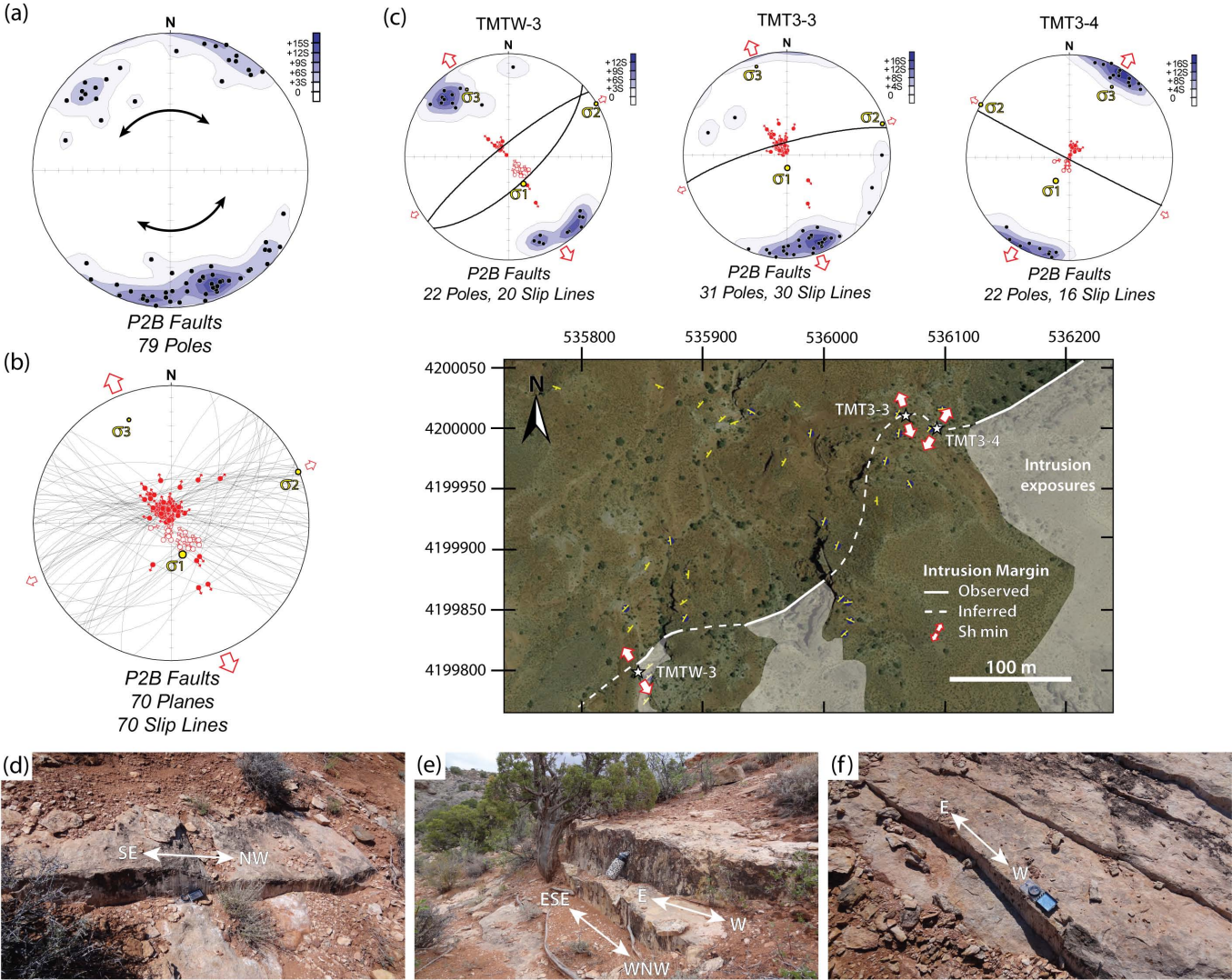
(a)
N
+15S
+12S
+9S
+6S
+3S
0
P2B Faults
79 Poles
(b)
N
σ3
σ2
σ1
P2B Faults
70 Planes
70 Slip Lines
(c)
TMTW-3
N
σ3
σ2
σ1
+12S
+9S
+6S
+3S
0
P2B Faults
22 Poles, 20 Slip Lines
TMT3-3
N
σ3
σ2
σ1
+16S
+12S
+8S
+4S
0
P2B Faults
31 Poles, 30 Slip Lines
TMT3-4
N
σ2
σ3
σ1
+16S
+12S
+8S
+4S
0
P2B Faults
22 Poles, 16 Slip Lines
535800
535900
536000
536100
536200
4200050
4200000
4199950
4199900
4199850
4199800
N
TMT3-3
TMT3-4
TMTW-3
Intrusion
exposures
Intrusion Margin
Observed
Inferred
Sh min
100 m
(d)
SE
NW
(e)
ESE
E
W
WNW
(f)
E
W

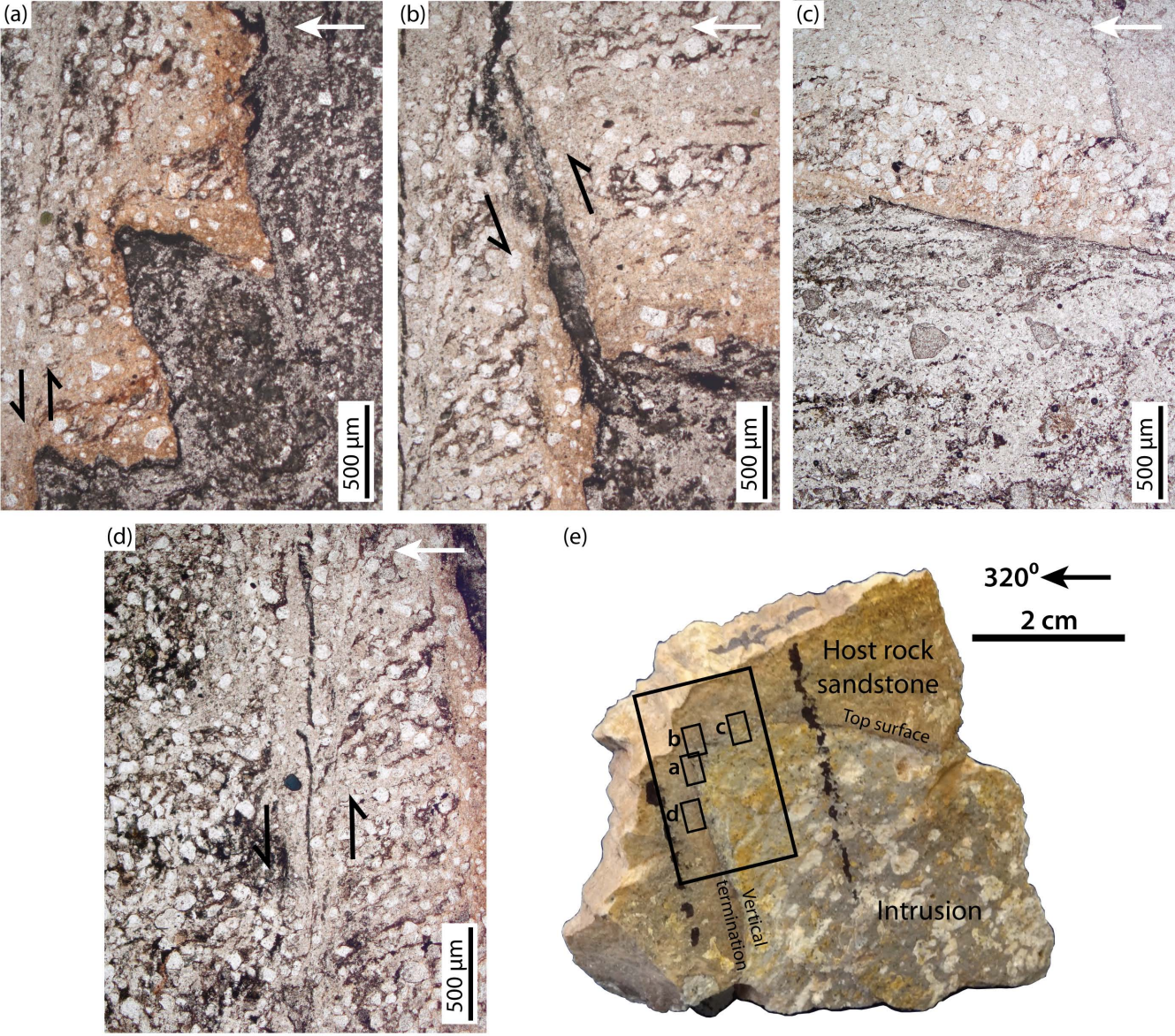
(a)
500 µm
(b)
500 µm
(c)
500 µm
(d)
500 µm
(e)
320°
2 cm
Host rock
sandstone
Top surface
b
c
a
d
Vertical
termination
Intrusion

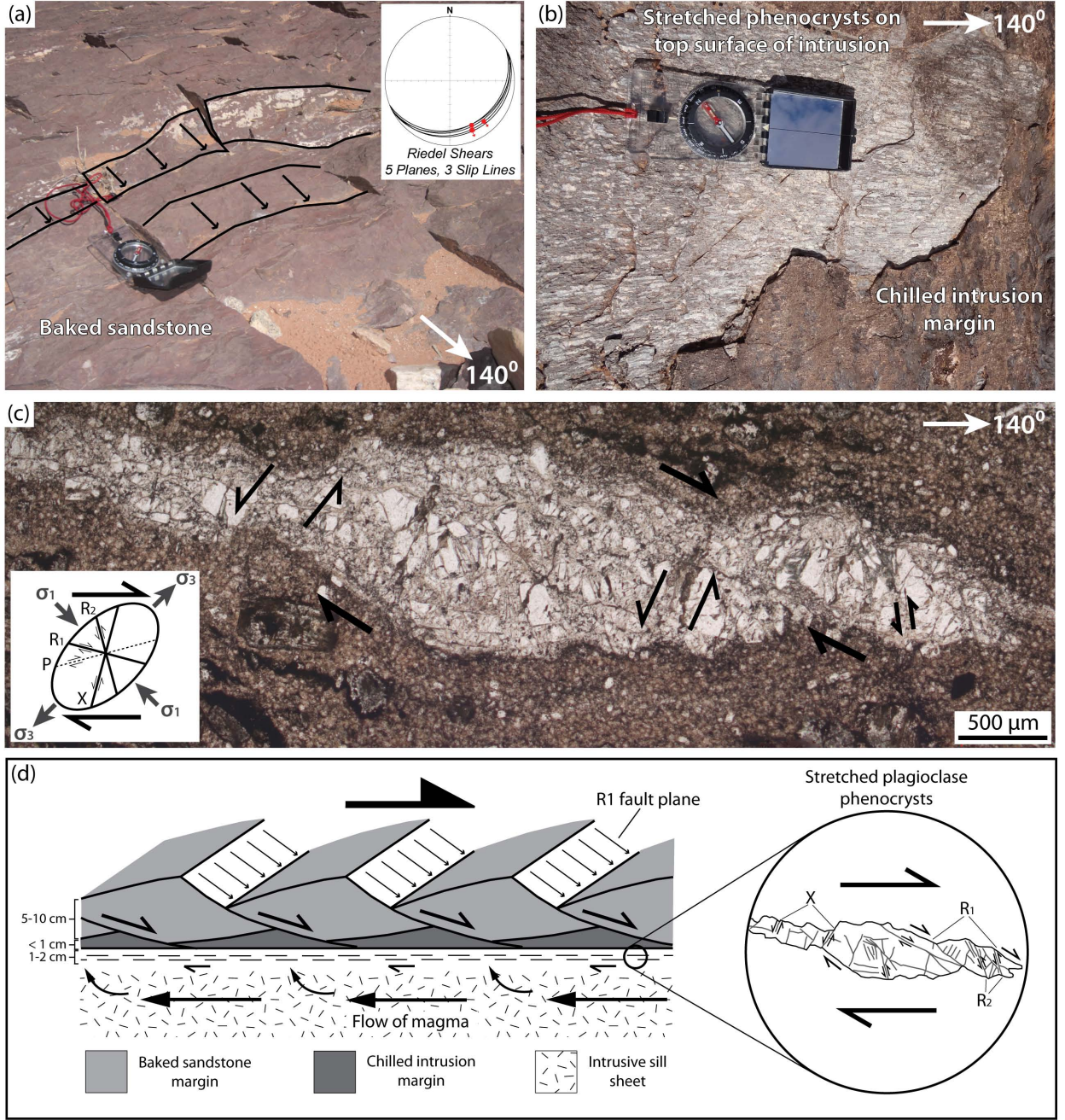
(a)
N
Riedel Shears
5 Planes, 3 Slip Lines
Baked sandstone
140⁰
(b)
Stretched phenocrysts on
top surface of intrusion
140⁰
Chilled intrusion
margin
(c)
140⁰
σ1
σ3
R2
R1
P
X
σ1
σ3
500 µm
(d)
R1 fault plane
Stretched plagioclase
phenocrysts
5-10 cm
< 1 cm
1-2 cm
Flow of magma
X
R1
R2
Baked sandstone
margin
Chilled intrusion
margin
Intrusive sill
sheet

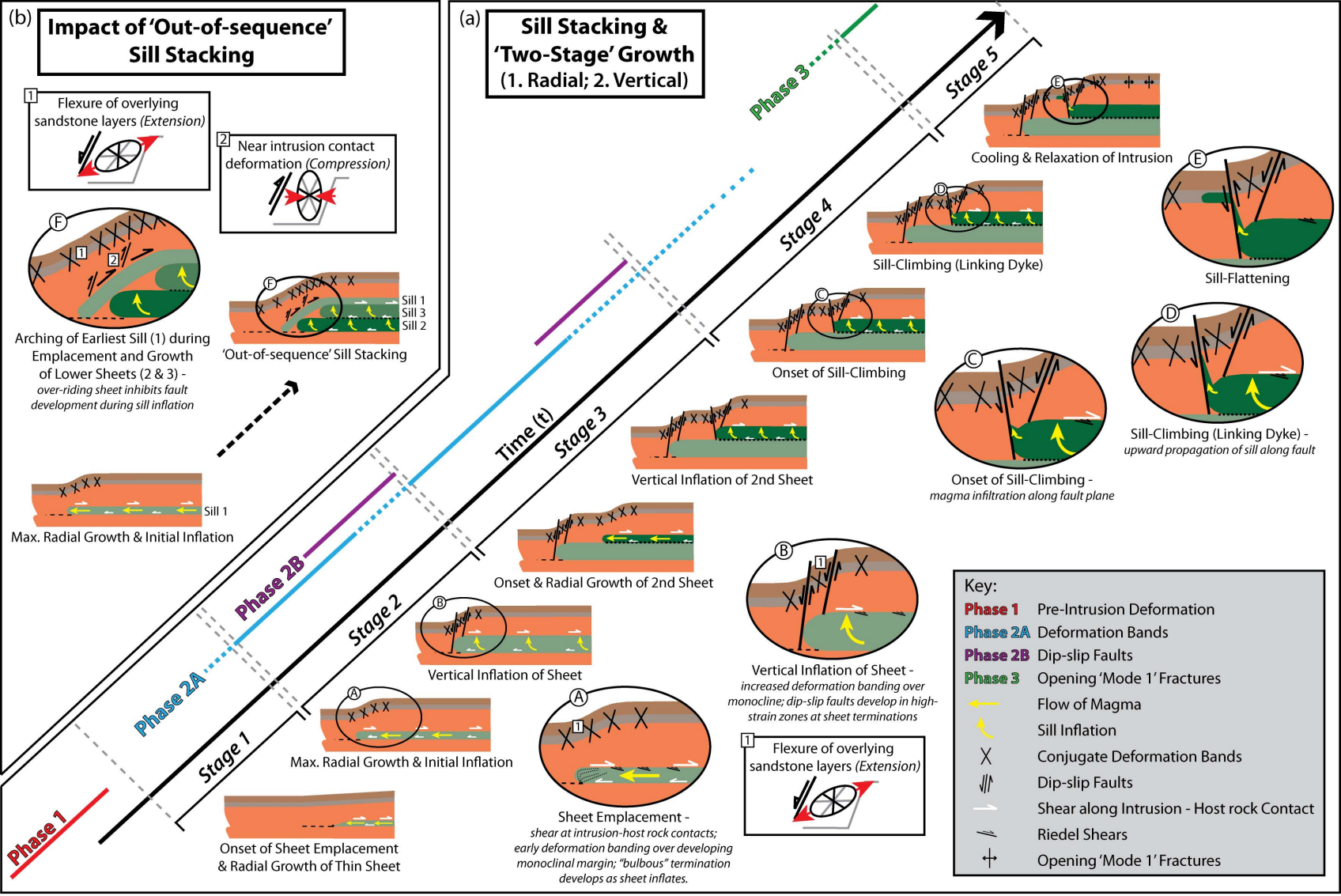
(b)
Impact of 'Out-of-sequence' Sill Stacking
1
Flexure of overlying sandstone layers (Extension)
2
Near intrusion contact deformation (Compression)
F
1
2
Arching of Earliest Sill (1) during Emplacement and Growth of Lower Sheets (2 & 3) -
over-riding sheet inhibits fault development during sill inflation
Sill 1
Sill 3
Sill 2
'Out-of-sequence' Sill Stacking
Sill 1
Max. Radial Growth & Initial Inflation
Phase 1
Phase 2A
Phase 2B
Phase 3
Stage 1
Stage 2
Stage 3
Stage 4
Stage 5
Time (t)
Onset of Sheet Emplacement & Radial Growth of Thin Sheet
A
Max. Radial Growth & Initial Inflation
B
Vertical Inflation of Sheet
Onset & Radial Growth of 2nd Sheet
Vertical Inflation of 2nd Sheet
C
Onset of Sill-Climbing
D
Sill-Climbing (Linking Dyke)
E
Cooling & Relaxation of Intrusion
(a)
Sill Stacking & 'Two-Stage' Growth
(1. Radial; 2. Vertical)
A
1
Sheet Emplacement -
shear at intrusion-host rock contacts; early deformation banding over developing monoclinal margin; "bulbous" termination develops as sheet inflates.
B
1
Vertical Inflation of Sheet -
increased deformation banding over monocline; dip-slip faults develop in high-strain zones at sheet terminations
C
Onset of Sill-Climbing -
magma infiltration along fault plane
D
Sill-Climbing (Linking Dyke) -
upward propagation of sill along fault
E
Sill-Flattening
1
Flexure of overlying sandstone layers (Extension)
Key:
Phase 1 Pre-Intrusion Deformation
Phase 2A Deformation Bands
Phase 2B Dip-slip Faults
Phase 3 Opening 'Mode 1' Fractures
Flow of Magma
Sill Inflation
Conjugate Deformation Bands
Dip-slip Faults
Shear along Intrusion - Host rock Contact
Riedel Shears
Opening 'Mode 1' Fractures

(a)

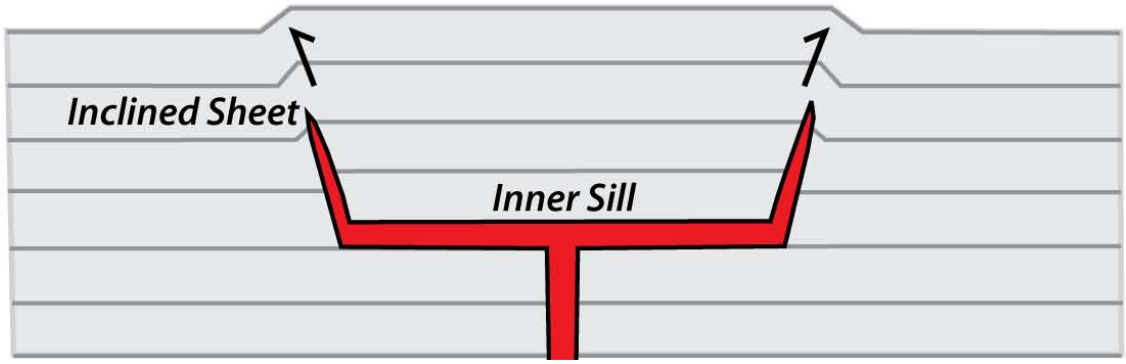

(b)

Stage 1 - Sheet propagation/ emplacement

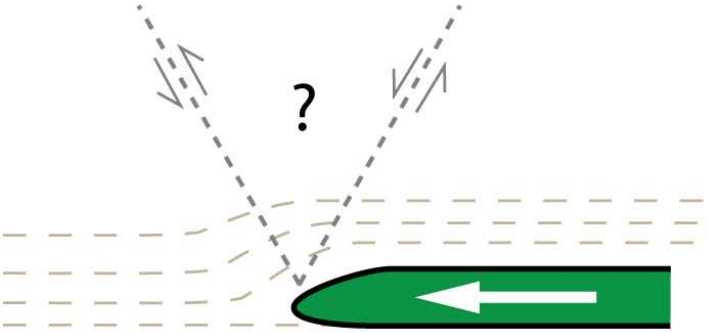

Initial emplacement of thin sill sheet.
Bedding moderately deformed by flexure and distributed deformation.
No faults developed.

Stage 2 - Sheet Inflation

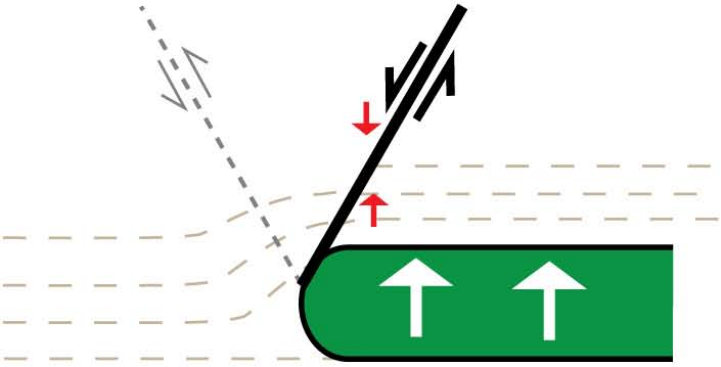

***Deformation localised** at sill tip.*
***Normal fault** develops.*
***No Sill climbing** (propagation of magma inhibited along fault due to vertical compressive stress associated with uplift of underlying HW block).*

or

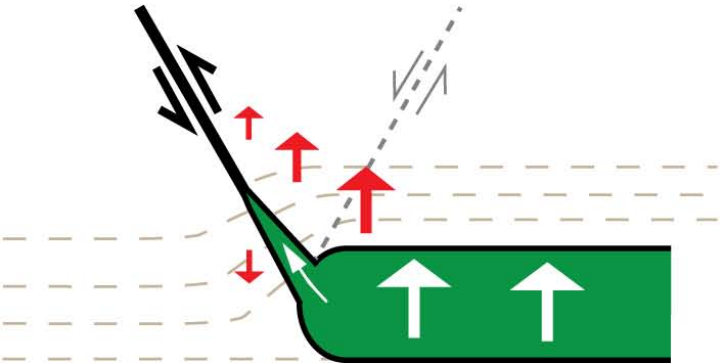

***Deformation localised** at sill tip.*
***Reverse fault** develops.*
***Sill climbing** (magma propagates along fault, exploiting void space created by uplift of HW block).*